LABORATORI NAZIONALI DI FRASCATI
SIS – Pubblicazioni

LNF-95/055 (IR)
25 Ottobre 1995

DAΦNE Exotic Atom Research

The DEAR Proposal

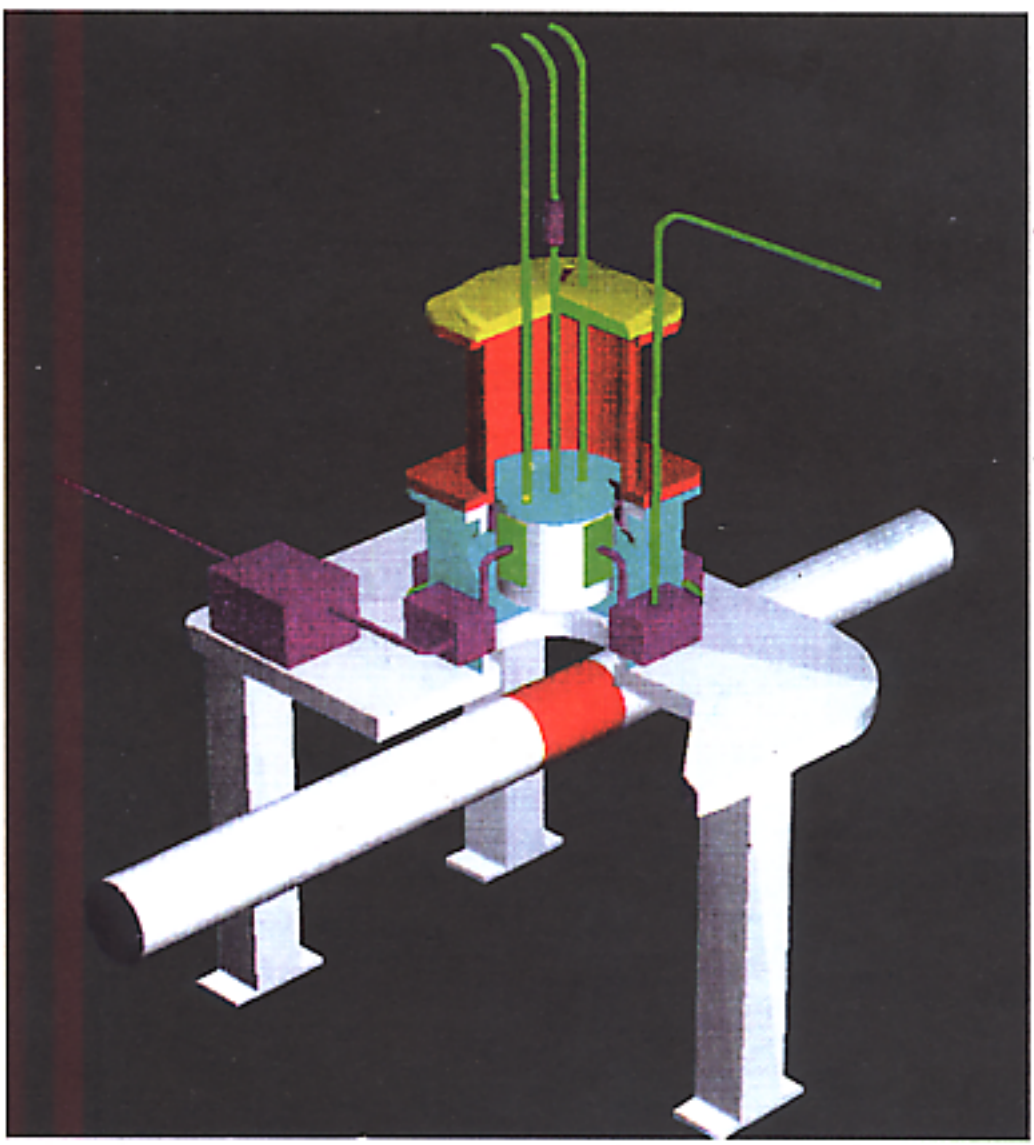

PACS.: 36.10.-k

The DEAR Collaboration

R. Baldini, S. Bianco, F.L. Fabbri, C. Guaraldo, V. Lucherini, C. Petrascu
Laboratori Nazionali di Frascati dell'INFN,
CP 13, Via E. Fermi 40, I-00044 Frascati (Roma), Italy

A. Vacchi, E. Zavattini
Univ. degli Studi di Trieste, Dip. di Fisica and INFN Sezione di Trieste,
Via A. Valerio 2, I-34127 Trieste, Italy

R. Jacot-Guillarmod, F. Mulhauser, L.A. Schaller, L. Schellenberg, H. Schneuwly
Inst. de Physique, Univ. de Fribourg,
Bd. de Pérolles, CH–1700 Fribourg, Switzerland

M. A. Augsburger, D. Chatellard, J.–P. Egger, E. Jeannet, D. Varidel
Univ. de Neuchâtel, Inst. de Physique,
1 rue A.–L. Breguet, CH–2000 Neuchâtel, Switzerland

A. Bragadireanu, M. Iliescu, T. Ponta, V. Zoran
Inst. of Atomic Physics (IFA), Dept. of High Energy Physics
PO Box MG-6, R–76900 Bucharest–Magurele, Romania

S.N. Nakamura
Inst. of Physical and Chemical Research (RIKEN),
2–1 Hirosawa, Wako, Saitama 351–01, Japan

T. Koike
Hokkaido Univ., Dept. of Physics,
N8W5 Kikta, Sapporo 060, Japan

R.S. Hayano, M. Hori, T. Ishikawa, T.M. Ito, M. Iwasaki
Univ. of Tokyo, Meson Science Lab. and Dept. of Physics,
7–3–1 Hongo, Bunkyo, Tokyo 113, Japan

Y. Akaishi
Univ. of Tokyo, Inst. for Nuclear Study
3–2–1 Midori, Tanashi, Tokyo 188, Japan

G. Beer
University of Victoria, Victoria, Canada

First Preface

" The most *important experiment* to be carried out in low energy K-meson physics today is the *definitive* determination of the energy level shifts in the K^-p and K^-d atoms, because of their direct connection with the physics of $\overline{K}N$ interaction and their complete independence from all other kinds of measurements which bear on this interaction".

R.H.Dalitz
Proc. Int. Conf. on "Hypernuclear and Kaon Physics",
Heidelberg 1982.

also cited by

C.J. Batty
Proc. Int. Conf. on "Intense Hadron Facilities and
Antiproton Physics", Torino 1990.

Second Preface

PHYSICAL REVIEW D

PARTICLES AND FIELDS

VOLUME 50

Third Series

1 AUGUST 1994

PART I

Review of Particle Properties

Baryon Full Listings

$\Lambda(1405)$

doubt its existence or quantum numbers. A measurement of the energy-level shifts and widths for the atomic levels of kaonic hydrogen (and deuterium) would give a valuable check on analyses of the $(\Sigma\pi, N\overline{K})$ amplitudes, since the energy of the K^-p atom lies roughly midway between those for the two sets of data. The three measurements of $(\Delta E - i\Gamma/2)$ for kaonic hydrogen are inconsistent with one another and require that the sign of $\mathrm{Re}(A_{I=0} + A_{I=1})$ be opposite that deduced from $N\overline{K}$ reaction data (see BATTY 89). Accurate measurements of $(\Delta E - i\Gamma/2)$ values for kaonic hydrogen are badly needed, but may not be possible until the KAON factory becomes operational.

To definitively settle the nature of the $\Lambda(1405)$ will require much further work, both experimental and theoretical. Higher-statistics experiments on the production and decay of the $\Lambda(1405)$ are needed, but suitable K^- beams will not be available until KAON. The low-energy reaction cross sections, especially for the $\overline{K}^0 p$ interactions, last studied 25 years ago, need to be better determined.

$\Lambda(1405)$

	Mode
Γ_1	$\Sigma\pi$
Γ_2	$\Lambda\gamma$
Γ_3	$\Sigma^0\gamma$
Γ_4	$N\overline{K}$

$\Lambda(1405)$ P

$\Gamma(\Lambda\gamma)$

VALUE (keV)	DOC
• • • We do not use the following data	
27±8	BU

$\Gamma(\Sigma^0\gamma)$

VALUE (keV)	DOC
• • • We do not use the following data	
10 ± 4 or 23 ± 7	BU

$\Lambda(1405)$ BR

$\Gamma(N\overline{K})/\Gamma(\Sigma\pi)$

VALUE	CL%	DO
• • • We do not use the following data		
<3	95	HE

$\Lambda(1405)$

Third Preface

The aim of this Proposal is to demonstrate the feasibility of an X-ray measurement on the kaonic hydrogen atom for the definitive determination of the energy level shift and width due to the $\overline{K}N$ strong interaction.
We intend to use the K^- from the ϕ's produced in the $DA\Phi NE$ machine; a low temperature pressurized hydrogen target; and a Charge-Coupled Device (CCD) detector. The reliability of the data that can be obtained from $DA\Phi NE$ is based on:

- the unique features, in terms of low momentum, high purity, medium intensity, which characterize the kaons from $DA\Phi NE$ with respect to any other existing kaon beam;

- the performance of CCD's, in terms of resolution and, above all, for background rejection capability, which make this device *the detector* for soft X-ray measurements in the background of an accelerator, as it has been demonstrated in these last years with the spectacular results obtained by CCD's in exotic atoms research at PSI (Villigen) and at LEAR (CERN);

- the use of a hydrogen target of moderate density, in order to reduce Stark mixing effects, which cause strong absorption of the kaon from high–n atomic s–states and to obtain a high statistics X–ray data sample.

Contents

Chapter 1

Exotic atoms and the kaon–nucleon interaction

1.1 Introduction

An "exotic atom" is formed when an incident negatively charged particle such as a muon, a pion, a K-meson, an antiproton or a Σ-hyperon, is stopped in a target and captured into a high atomic Bohr orbit around the nucleus, replacing one of the outer electrons and giving rise to a highly excited atom. The particle then cascades down through its own series of atomic levels, initially by Auger transitions, in which orbital electrons are ejected and in the later stages of the cascade by emission of X-rays. Finally, in the case of hadronic atoms, at some final n-value, nuclear absorption by the nucleus dominates, all hadrons reaching the level are captured and the X-ray series terminates.

The strong interaction causes a shifting of the energy of the lowest atomic level from its purely electromagnetic value, whilst the absorption reduces the lifetime of the state and so X-ray transitions to this final atomic level are broadened. Precise measurements of the X-ray energy spectrum then allow the energy shift (ϵ) and width (Γ) associated with this final level to be determined. As the atomic number and size of the nucleus increase, the absorption occurs from higher n–values. For example, in kaonic hydrogen transitions to n=1 states (K series) have been observed; in light nuclei such as He, Li, Be, etc. the transitions terminate at n=2, whereas in heavy nuclei such as Pb or U the X-ray series finishes at n=7.

In order to determine the energy shift ε, the electromagnetic energy of the unshifted line must first be calculated. This is usually obtained by solving the Klein-Gordon wave equation using the Coulomb potential obtained from a realistic nuclear charge distribution. Other corrections can be calculated using second–order perturbation theory and include first and higher order vacuum polarization, electron screening, relativistic corrections to the reduced mass approximation, nuclear polar-

ization and the Lamb shift. Depending on the energy of the level to be calculated and on the magnitude of the various corrections, the electromagnetic energy can usually be calculated to an accuracy of a few electron volts.

In Table 1 the calculated electromagnetic level energies for kaonic hydrogen and kaonic deuterium are reported.

Table 1

Kaonic hydrogen and deuterium level energies (KeV)

Line	kaonic hydrogen	kaonic deuterium
K_α	6.46	7.81
K_β	7.66	9.26
K_γ	8.07	9.79
$K^{}$	8.61	10.41

The energy shift (ε) and width (Γ) of the $1s$ level in kaonic hydrogen, measured from the $2p$ - $1s$ X–ray transition, can be related in a fairly model independent way to the real and imaginary part of the complex s-wave $K^- p$ scattering length a_{K^-p}: to first order in $\mu\alpha\, a_{K^-p}$

$$\varepsilon + \frac{i}{2}\Gamma = 2\alpha^3\mu^2\, a_{K^-p} = 412\, a_{K^-p}\, eV\, fm^{-1}$$

with μ reduced mass, α fine structure constant. This expression is known as the Deser-Trueman formula [1].

As far as experiments are concerned, collisional effects in the atomic cascade due to Stark mixing and external Auger transitions are important and the yield of X–rays decreases with increasing target density. This is a particular problem for kaonic hydrogen experiments, where high density targets are required to reduce the path of the kaon and hence the probability of kaon decay during the processes of stopping, atomic capture and atomic cascade. A compromise between number of stopped kaons in a reasonable volume and yield of $2p$ - $1s$ X–rays has to be carefully looked by varying the density of a gaseous target through its pressure and temperature parameters.

1.2 The kaon–nucleon interaction at low energies

The $\overline{K}N$ interaction at low energies has *rich, complex dynamical aspects*, which are *neither simple nor well understood.* Not simple, since the K^-p and $\overline{K}^0n$ channels are coupled by charge exchange and, furthermore, are strongly coupled to several πY channels ($Y = \Lambda, \Sigma$) open at the K^-p threshold (1432 MeV total energy in the centre of mass):

$$K^-p \rightarrow K^-p$$
$$K^-p \rightarrow \overline{K}^0n \; - 5\, MeV$$
$$K^-p \rightarrow \pi\Sigma \; + 100\, MeV$$
$$K^-p \rightarrow \pi^0\Lambda \; + 180\, MeV$$

Moreover, this energy region is dominated by the presence of the s-wave $\Lambda\,(1405)$ resonance, a strangeness -1, $I = 0$ resonance which decays only to $\Sigma\pi$. This resonance also couples strongly to the $\overline{K}N$ system, but does not decay to it since it is some 30 MeV below the $\overline{K}N$ threshold.

Resonances occur also in other partial waves above (the $\Lambda(1520)$ in d-wave) and below (the $\Sigma(1385)$ in p-wave) threshold.

Experimental data are available for:

a) the K^-p cross sections for the elastic and inelastic processes;

b) the three branching ratios for the K^-p absorption at rest[2]:

$$\gamma = \lim_{k\to 0} \frac{\sigma(K^-p \rightarrow \pi^+\Sigma^-)}{\sigma(K^-p \rightarrow \pi^-\Sigma^+)} = 2.36 \pm 0.04$$

$$R_c = \lim_{k\to 0} \frac{\sigma(K^-p \rightarrow charged\ particle)}{\sigma(K^-p \rightarrow all\ final\ states)} = 0.664 \pm 0.011$$

$$R_n = \lim_{k\to 0} \frac{\sigma(K^-p \rightarrow \pi^0\Lambda)}{\sigma(K^-p \rightarrow all\, neutral\, states)} = 0.189 \pm 0.015$$

c) the $\pi\Sigma$ invariant mass distribution below the K^-p threshold, which exibits the $\Lambda(1405)$ resonance;

d) the $1s$ level shift of the K^-p atom determined through X-ray measurements.

1.2.1 The scattering data

The data for a)–c), with varying degrees of accuracy, became available in the 1950s through the 1970s. The data on a) were (and still are) available only for about 1440 MeV and above in the center of mass energy of the K^-p system.

Analyses have usually been made by using a K-matrix formulation with the assumption that its matrix elements are smooth functions of energy, thus allowing extrapolation down to threshold and below to describe the multichannel problem. A constant scattering length approach was used in early analyses, equivalent to neglecting the variation in the final state momentum. Energy dependences were then allowed in subsequent zero-range and finite-range K-matrix analyses and in some cases waves higher than *s*-wave were included, so as to exploit also high energy data. The constraint to the K-matrix analysis that the $\pi\Sigma$ mass spectrum obtained from the $\pi^-p \rightarrow \pi\Sigma K$ reaction should be fitted simultaneously with data above threshold was added, in order to better determine the parameters of the $\Lambda(1405)$. Dispersion relations turned out to give powerful constraints on the analysis of low energy K^-p data.

No particular disharmony was noticed among data. The $\overline{K}N$ scattering lengths were determined in this way [4]÷[5].
The K^-p scattering length a_{K^-p} is deduced by the isospin average:

$$a_{K^-p} = \frac{1}{2}(a_0 + a_1)$$

where a_0 and a_1 are the scattering lengths for the channels I=0, 1. In Table 2 results of $\overline{K}N$ scattering analyses are reported. Common distintive feature of the measured scattering lengths, obtained by considering cross sections, branching ratios at threshold and $\pi\Sigma$ invariant mass distribution, is the *negative value of the real part of* a_{K^-p}:

$$Re\, a_{K^-p} < 0$$

Table 2

S-wave $\overline{K}N$ scattering lengths (fm)

Reference	I = 0		I = 1	
	a_0	b_0	a_1	b_1
Sakitt *et al.* (1965)	- 1.63±0.07	0.51±0.05	- 0.19±0.08	0.44±0.04
Kim *et al.* (1967)	- 1.67±0.04	0.71±0.04	- 0.07±0.06	0.68±0.03
von Hippel *et al.* (1968)	- 1.65±0.04	0.73±0.02	- 0.13±0.02	0.51±0.03
Martin & Ross (1970)	- 1.74±0.04	0.70±0.01	- 0.05±0.04	0.63±0.06
Martin *et al.* (1981)	- 1.70±0.07	0.68±0.04	0.37±0.09	0.60±0.07

This means, from the Deser-Trueman formula, and the Warsaw convention [8], that the *energy shift* due to the strong interaction turns out *negative*:

$$\epsilon < 0$$

i.e. the strong interaction is *repulsive* and shifts the electromagnetic level to a *less bound energy*. Hadronic shifts and widths obtained from the scattering lengths given by the analyses of scattering data[4]÷[5]are reported in Table 3.

Table 3

The energy shift ΔE_{1S} and width Γ_{1S} of the K^-p 1S state as obtained from kaonic hydrogen X-ray measurements and scattering analyses

Method	Experiment	ΔE_{1S} (eV)	Γ_{1S} (eV)
Kaonic hydrogen X-ray measurements	Davies *et al.* (1979)	$+40 \pm 60$	$0\ ^{+230}_{-0}$
	Izycki *et al.* (1980)	$+370 \pm 80$	560 ± 80
	Bird *et al.* (1983)	$+193 \pm 60$	$80\ ^{+220}_{-80}$
K^-p *scattering analyses*	Sakitt *et al.* (1965)	-375 ± 21	396 ± 25
	Kim *et al.* (1967)	-358 ± 16	568 ± 25
	von Hippel *et al.* (1968)	-367 ± 8	511 ± 16
	Martin & Ross (1970)	-367 ± 12	544 ± 25
	Martin *et al.* (1981)	-272 ± 21	527 ± 33

In addition to the data a)–c) there are data on the Coulomb–nuclear interference in the K^-p scattering at higher energies, i.e., for E$\geq$1500 MeV. When extrapolated to low energies, also these data were found to be consistent with $Re\, a_{K^-p} < 0$ [9].

1.2.2 The "kaonic hydrogen puzzle"

The three published X-ray experiments have all used liquid hydrogen targets and one or more Si(Li) detectors to measure X-ray transitions. Davies *et al.*[10] observed a 2σ peak at 6.52$\pm$0.06 KeV, which they attributed to the $2p$ - $1s$ X-ray. Izycki *et al.*[11] observed a weak pattern of 3 lines at 6.96$\pm$0.09, 7.99$\pm$0.07 and 8.64$\pm$0.10 KeV with significance 2σ, 3σ and 2σ, which they assigned to the $2p$, $3p$ and $4p$ - $1s$ transistions. On the other hand Bird *et al.*[12] saw a similar series of three lines with significance σ, 3σ and 0.5 σ.

It is difficult to interpret and reconcile the X-ray spectra measured by these three experiments. For example, in the experiment of Davies *et al.*[10] the single peak only

It is difficult to interpret and reconcile the X-ray spectra measured by these three experiments. For example, in the experiment of Davies *et al.*[10] the single peak only shows up clearly in the spectrum where the background has been reduced by selecting a particular time region of pulses from the detector. Izycki *et al.*[11] claim a very large detector acceptance by using a target which is not much larger than the beam size and with the detectors very close to the beam. Finally, the X-ray lines measured by Bird *et al.*[12] were only observed in the first part of the experimental run. In the later stages of the experiment only a rather smooth spectrum was measured.

The measured values are generally inconsistent with each other at least as far as the magnitude of the strong interaction shift ε is concerned, *however they are all in agreement about the sign of* ε:

$$\varepsilon > 0\,,$$

as reported in Table 3. This means that the hadron interaction of the kaon shifts the atomic level to a more bound energy, in direct contradiction with the repulsive strong interaction found from scattering data analyses. It follows, from the Deser–Trueman formula, that X-rays emitted in transitions to the $1s$ level of kaonic hydrogen give a *positive sign for the real part of the scattering length*

$$Re\, a_{K^-p} > 0$$

whilst the real part of the K^-p scattering length obtained from K–matrix analyses of scattering data turns out negative. Table 4 contains the scattering lengths obtained from X-ray measurements [10]÷[12].

Table 4

The K^-p scattering lengths determined from kaonic hydrogen X-ray measurements and those from scattering analyses

Method	Reference	a_{K^-p} (fm)
Kaonic hydrogen	Davies *et al.* (1979)	$(0.10\pm0.14) + i(0.00\ ^{+0.28}_{-0.00})$
X-ray measurements	Izycki *et al.* (1980)	$(0.65\pm0.19) + i(0.68\pm0.31)$
	Bird *et al.* (1983)	$(0.47\pm0.14) + i(0.10\ ^{+0.27}_{-0.10})$
K^-p *scattering analyses*	Sakitt *et al.* (1965)	$(-0.91\pm0.05) + i(0.48\pm0.03)$
	Kim *et al.* (1967)	$(-0.87\pm0.04) + i(0.69\pm0.03)$
	von Hippel *et al.* (1968)	$(-0.89\pm0.02) + i(0.62\pm0.02)$
	Martin & Ross (1970)	$(-0.89\pm0.03) + i(0.66\pm0.03)$
	Martin *et al.* (1981)	$(-0.66\pm0.05) + i(0.64\pm0.04)$

The striking discrepancy between scattering data and X-ray measurements, apparent in Table 3 and 4, is often referred to as the *"kaonic hydrogen puzzle"*.

1.2.3 Corrections to scattering length

There are two principal corrections to the isospin average formula for the scattering length. The first takes into account the threshold difference between the $\overline{K}p$ and $\overline{K}^0 n$ channels, the second considers the Coulomb correction. In Table 5 the results of the corrections for threshold effects for zero range interaction[13] and for finite range interaction[14] are reported. Two different treatments of Coulomb corrections are also reported[15],[16].

Table 5

Corrections to scattering lengths

Correction	Scattering Length (fm)	ε (eV)	Γ (eV)
Isospin average $a_s = (a_0 + a_1)/2$	- 0.655 + i 0.705	- 270 (-268	581 611)
Including threshold effects a_t for zero range interaction (Dalitz and Tuan)	- 0.995 + i 0.827	- 410 (-414	682 736)
Including threshold effects in finite range interaction a_{BG} (Batty and Gal)	- 0.945 + i 785	- 389 (-393	647 692)
Coulomb correction a_{DT} (Dalitz and Tuan)	- 0.963 + i 0.702	- 397 (-404	579 620)
Coulomb correction a_W (Wycech)	- 0.961 + i 0.683	- 396 (-402	562 606)

As it is seen from the table, threshold effects give a marked change in the value of the scattering length, the real part increasing by about 50% and the imaginary part by 20%. Inclusion of Coulomb corrections to the threshold corrected value, using either the Dalitz[15] or the Wycech[16] approach, gives similar results.

Higher order terms to the Deser-Trueman formula were also considered by Trueman[1] and by Stepien–Rudzka and Wycech[16]. To second order, the effect on ε is seen to be small, whilst the values of Γ are typically increased by 10% (values in parentheses in Table 5).

1.3 The importance of an X-ray measurement on kaonic hydrogen

We discuss now the scientific meaning of an X–ray measurement on kaonic hydrogen.

X–rays given off in transitions to the $1s$ level of kaonic hydrogen show that the nuclear interaction of the kaon is of attractive nature and therefore gives rise to a more bound system[10]÷[12]. This is a puzzle, in that the hadronic shift is in a direction opposite to that calculated[17]÷[19] with the use of the analyses of low-energy $\overline{K}N$ experiments[4]÷[5], [20]÷[26]. It is also opposite to the shift observed in heavier kaonic atoms[8], in which again the interaction turns out repulsive. Unraveling this puzzle is therefore crucial for an understanding of the kaon–nucleon interaction. Moreover, since for the kaon-proton system at threshold the energy region is dominated by the presence of the $\Lambda(1405)$ resonance, the structure of this object can be investigated. Indeed, whether the $\Lambda(1405)$ is composite ($\overline{K}N$ bound state or $\Sigma\pi$ resonance) or is elementary (three–quark state) or is a $\overline{K}N$ bound state with an admixture of three quark–state is controversial[27]÷[31].

In the simplest analysis, the atomic level shift and width are related to scattering data via the proportionality expressed by the Deser–Trueman formula[1]. Since corrections to the formula found in exact calculations [18,19,32] are large, but not large enough to reverse the sign of ϵ, the problem must be with either experiments or the behaviour of the scattering amplitude around threshold. As we have seen, corrections to the scattering length substantially do not change the value obtained analyzing the scattering data, hence attention has to be paid to X-ray measurements. Here the situation is actually confused on the experimental point of view.

The quality of the existing X-ray data has been already discussed: high background, which is not surprising since this is typical of a hadron beam which has to be degraded; large statistical errors; suspected systematic errors; inconsistencies among the results. However, the X–ray data agree at least on one point – that $Re\, a_{K^-p}$ is positive, so a discrepancy with scattering data exists.

To confirm this result, mainly as far as sign is concerned, but giving also a precise determination of the magnitude of shift and width, is the reason why a new experiment,with high resolution, good background rejection and high statistics, is badly needed. Once more, it is useful to recall that X-ray results represent the *only* direct experimental evidence on the near-zero-energy $\overline{K}N$ interaction. Hence, the strong statement of Dalitz, that we reported in the First Preface, according to which *the most important experiment to be carried out in low energy K–meson physics today is the definitive determination of the energy level shift in the K^-p and K^-d atoms.*

The M- and K-matrix analyses extrapolate scattering data (cross sections and

amplitudes determined by Coulomb-nuclear interference) measured at higher energies down to threshold and below. The X-ray experiment calls this extrapolation into question. For a nearly attractive interaction, $Re\, f_{K^-p}$ starts out positive at threshold and reverses sign each time the strength of the interaction increases to the point where it supports another subthreshold bound state (see fig. 1). Accordingly, *the sign and magnitude of Re f deduced from the shift in kaonic hydrogen are related to the existence and nature of subthreshold states.*

Thus the puzzle centers on the energy dependence of the scattering amplitude $f_{K^-p}(E)$ in the region from the Coulomb bound state (8 KeV below threshold) to the low end of the scattering data (5 MeV above threshold). Note these energy differences: here lies the capability of a better investigation and understanding of the $\overline{K}N$ interaction diplayed by X–ray measurements, which do not need any extrapolation to zero–energy.

Along this line, several attempts to reconcile scattering data and energy shift measurements have been made so far: see for instance[34]$\div$[42]. We shall give two significant examples, chosen in order to show the role played by the $\Lambda(1405)$ and also that of quark degrees of freedom in the $\overline{K}N$ interaction.

The Kumar and Nogami model[41] assumes that there is an "elementary" baryon Λ_0, which has the same quantum numbers as $\Lambda(1405)$ and a mass near the K^-p threshold (1432 MeV). The Λ_0 could be a three–quark state which is as elementary as the nucleon. The Λ_0 is a "bare" particle which can not be observed directly, but it causes the observed resonance $\Lambda(1405)$. The relevant fact is that *the presence of* Λ_0 *leads to a rapid variation of the* K^-p *scattering length around threshold* such that the apparent contradiction between the atomic level shift and the scattering data could be avoided. More specifically, Kumar and Nogami assumed that the K^-p amplitude f_{K^-p} is dominated by the I=0 component and in the model the $\overline{K}N$ isosinglet amplitude f_0 satisfies the following conditions:

i) $Re\, f_o \simeq 0$ at threshold,

ii) $Re\, f_o$ vanishes at E=1405 MeV, *implying an unstable bound state* $\overline{K}N$ (see fig.1.1).

From the model, $a_{K^-p} \geq 0$, which is consistent with the atomic data. However, the model is not complete, since it does not attempt to fit all available data, such as the branching ratios at threshold [2].

The Tanaka and Suzuki model[42] assumes directly a central hypothesis consistent with the atomic data, i.e. $Re\, a_{K^-p} > 0$ at threshold. All the four "categories" of experimental data a)$\div$d) are fitted without the need of an "elementary" three–quark state such as the Λ_0. Therefore, the $\Lambda(1405)$ is simply a two–body composite system and one is led to ask whether or not the $\Lambda(1405)$ is a $\overline{K}N$ bound state rather

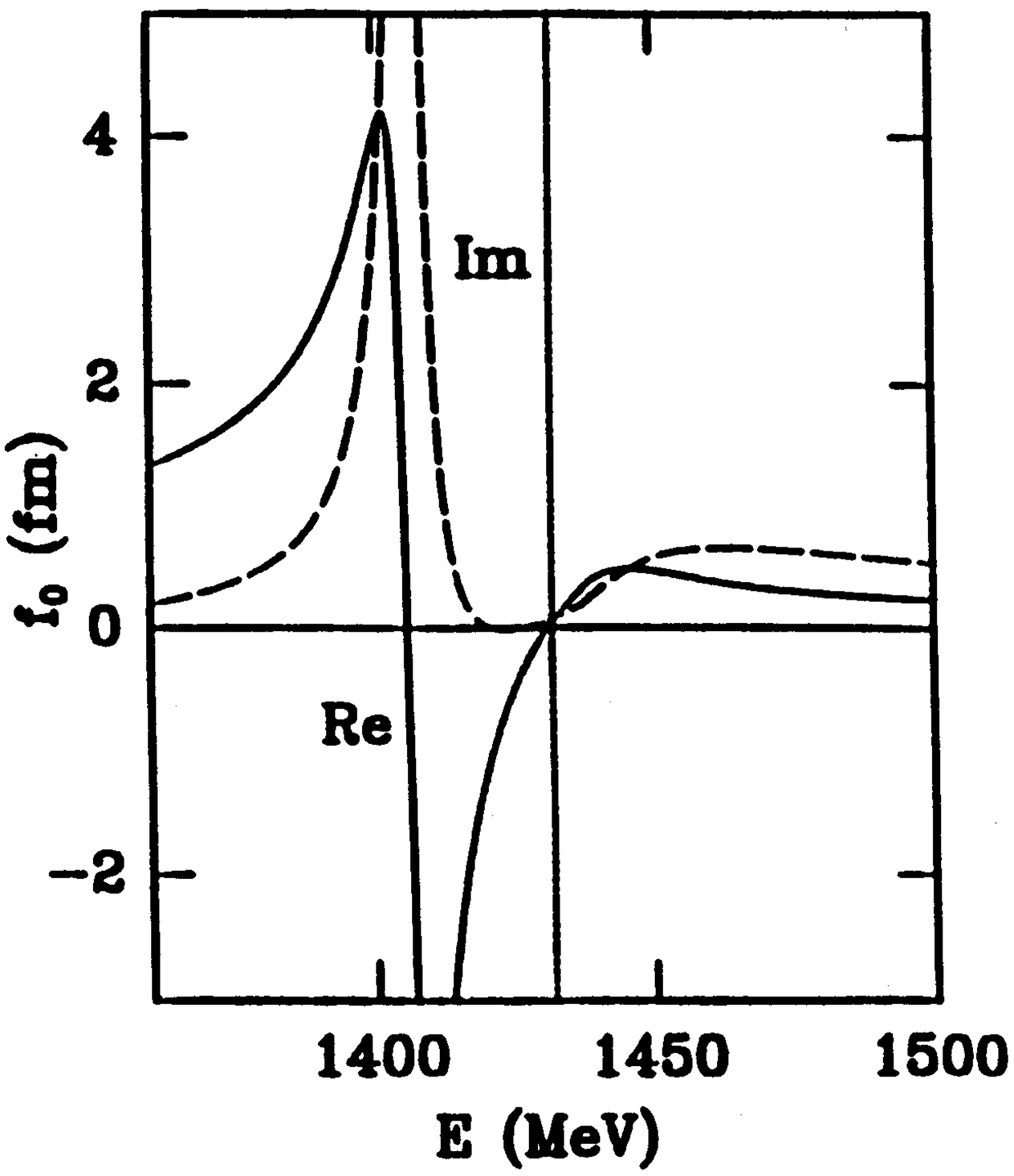

Figure 1.1: The $\overline{K}N$ isosinglet amplitude f_0 versus the total c.m. energy. The solid and dashed lines represent the real and imaginary part, respectively, of the amplitude. The vertical line shows the $\overline{K}p$ threshold (1432 MeV)

than a $\pi\Sigma$ resonance. It is of course conceivable that the $\overline{K}N$ and $\pi\Sigma$ channels are coupled so strongly that there is no clear answer to this question. However, the model provides some insight into this aspect. Indeed the $Re\, f_{K^-p}$ is positive around threshold but the real part of the I=0 component of the amplitude, $Re\, f_o$, vanishes and changes its sign below the $\overline{K}N$ threshold. This implies that there is an unstable bound state of $\overline{K}$ and N in the isosinglet state. In this sense, $\Lambda(1405)$ is an unstable bound state of $\overline{K}$ and N.

Summarizing, good data (in terms of statistics, low background, good resolution) from kaonic hydrogen X–ray measurements will allow:

- understanding the antikaon–nucleon interaction, in particular by definitively solving the "kaonic hydrogen puzzle";
- understanding the nature of the $\Lambda(1405)$ and therefore testing also the prediction of the quark model;
- clarifying the behaviour with energy around threshold of the scattering amplitude f_{K^-p};

and, moreover,

- studying the influence of quark configurations on the spectrum of hadronic atoms;
- understanding astrophysical implications, like kaon–condensation in dense neutron star matter[40].

Bibliography

[1] S. Deser *et al.*, Phys. Rev. **96** (1954) 774;
T.L. Trueman, Nucl. Phys. **26** (1961) 57;
A. Deloff, Phys. Rev. **C13** (1976) 730.

[2] D.N. Tovee *et al.*, Nucl. Phys. **B33** (1971) 493;
R.J. Nowak *et al.*, Nucl. Phys. **B139** (1978) 61;
J. K. Kim, Columbia University Report, Nevis 149 (1966).

[3] M. Sakitt *et al.*, Phys. Rev. **B139** (1965) 719.

[4] J.K. Kim, Ph.D. Thesis Columbia University, Nevis **149** (1966);
J.K. Kim, Phys. Rev. Lett. **19** (1967) 1074.

[5] F.von Hippel and J.K. Kim, Phys Rev. Lett. **20** (1968) 1303.

[6] A.D. Martin and G.G. Ross, Nucl. Phys. **B16** (1970) 479.

[7] A.D. Martin, Nucl. Phys. **B179** (1981) 33.

[8] C.J. Batty, Nukleonika **25** (1980) 545.

[9] P. Baillon *et al.*, Nucl. Phys. **B105** (1976) 365.

[10] J.D. Davies *et al.*, Phys. Lett. **B83** (1979) 55.

[11] M. Izycki *et al.*, Z. Phys. **A297** (1980) 11.

[12] P.M. Bird *et al.*, Nucl. Phys. **A404** (1983) 482.

[13] R.H. Dalitz and S.F. Tuan, Ann. Phys. **10** (1960) 307.

[14] C.J. Batty and A. Gal, Il Nuovo Cimento **102A** (1989) 255.

[15] R.H. Dalitz and S.F. Tuan, Ann. Phys. **10** (1960) 307;
A. Deloff and J. Law, Phys. Rev. **C20** (1979) 1597.

[16] W. Stepien–Rudzka and S. Wycech, Nukleonika **22** (1977) 929.

[17] R. C. Barrett, J. Phys. **G9** (1983) 355.

[18] R. H. Landau, Phys. Rev **C 28** (1983) 1324;
R.H. Landau and B. Cheng, Phys. Rev. **C 33** (1986) 734.

[19] J. Thaler, J. Phys. **G10** (1984) 1037.

[20] W. E. Humphrey and R. R. Ross, Phys. Rev. **127** (1962) 1305.

[21] W. Kittel, G. Otter and I. Wacek, Phys. Lett. **21** (1966) 349.

[22] T.S. Mast *et al.*, Phys. Rev. **D11** (1975) 3078.

[23] T.S. Mast *et al.*, Phys. Rev. **D14** (1976) 13.

[24] R.O. Bangerter *et al.*, Phys. Rev. **D23** (1981) 1484.

[25] J. Ciborowski *et al.*, J. Phys. **G8** (1982) 13.

[26] D. Evans *et al.*, J. Phys. **G9** (1983) 885.

[27] R.H. Dalitz and J.G. McGinley, in *Low and Intermediate Energy Kaon–Nucleon Physics*, edited by E. Ferrari and G. Violini (Reidel, Boston, 1981), p. 97.

[28] S. Capstick and N. Isgur, in *Hadron Spectroscopy–1985*, edited by S. Oneda, AIP Conference Proceedings No. 132 (American Institute of Physics, New York, 1985), p. 267.

[29] E. A. Veit, B. K. Jennings, A. W. Thomas and R. C. Barrett, Phys. Rev. **D 31** (1985) 1033.

[30] B. K. Jennings, Phys. Lett. **176 B** (1986) 229.

[31] K. Maltman and N. Isgur, Phys. Rev. **D 34** (1986) 1372.

[32] H.H. Brouwer, J.W. de Maag and L.P. Kok, Z. Phys. **A 318** (1984) 1.

[33] K.S. Kumar *et al.*, Z. Phys. **A304** (1982) 301.

[34] B.O. Kerbikov, Pis'ma Zh. Eksp. Teor. Fiz. **37** (1983) 118.

[35] B.O. Kerbikov, Yad. Fiz. **41** (1985) 725.

[36] J. Schnick and R.H. Landau, Phys. Rev. Lett. **58** (1987) 1719.

[37] P. Y. Fink *et al.*, Phys. Rev. **C41** (1990) 2720.

[38] G. He and R. M. Landau, Phy. Rev. **C48** (1993) 3047.

[39] E. Friedman, A. Gal and C. J. Batty, Phys. Lett. **B308** (1993) 6.

[40] C.–H. Lee *et al.*, Phys. Lett. **B326** (1994) 14.

[41] K.S. Kumar and Y. Nogami, Phys. Rev. **D21** (1980) 1834.

[42] K.Tanaka and A. Suzuki, Phys. Rev. **C45** (1992) 2068.

Chapter 2

The DEAR experimental set-up

2.1 The principle of the experiment

The principle of the DEAR experiment is very simple: the low momentum negative kaons produced by decay of ϕ's, created by e^+e^- collisions in the interaction point of one of the straight sections of DAΦNE, leave the beam pipe through a thin window, are degraded in energy down to few MeV, enter a hydrogen target placed few centimeters above the pipe and are there stopped. A fraction of kaons is captured in an outer orbit of the hydrogen atom, thus forming an exotic atom. The kaon then cascades down through its own series of bound atomic states until it reaches a level where the short-range strong interaction acts on the particle causing its absorption.

Measuring, with a suitable soft X-ray detector, such as a Charge–Coupled Device (CCD), the last X-ray transition (the $2p$–$1s$ in kaonic hydrogen), allows one to obtain the shift of the $1s$ level caused by the $\bar{K}N$ strong interaction.

A $3D$ pictorial view of the proposed experimental set-up is shown in fig. 2.1.

2.2 The overall set-up

The DEAR experimental set-up has been designed taking into account the characteristics of the DAΦNE "kaon beam": low momentum (127 MeV/c), K^- emitted with a $sin(\theta)^2$ law (where θ is the angle measured respect to the beam pipe axis), all around the pipe.

The target has been placed at $\theta = 90°$, and the degrader, window thickness, and target density have been selected in order to optimize, on one hand the number of stopped kaons, and on the other the detected X-rays. Moreover, the set-up has to allow the use of very thin windows between the target volume containing gaseous hydrogen and the CCD detectors, described in Chapter 3, which are located all

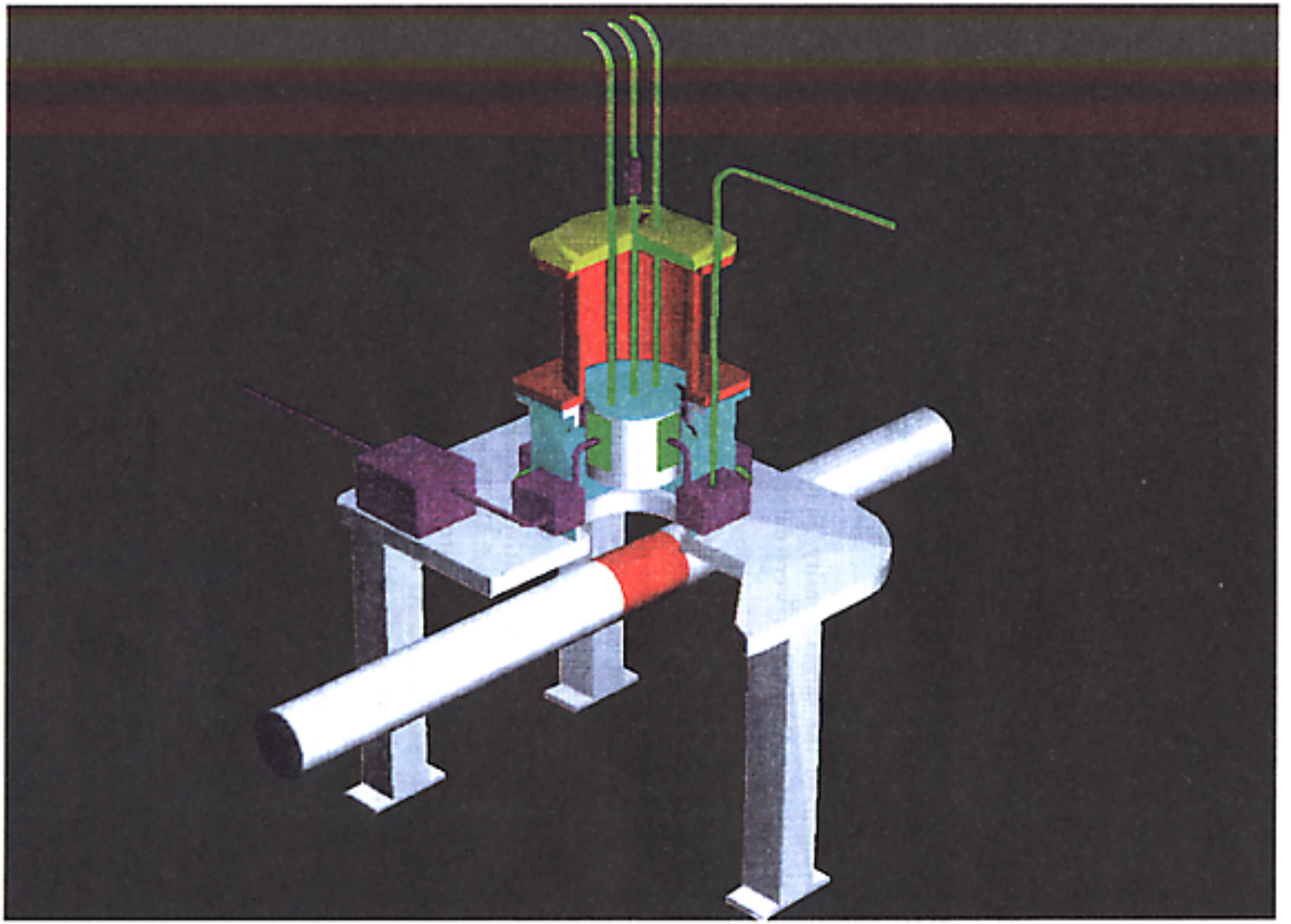

Figure 2.1: Pictorial $3D$ view of the proposed experimental set-up for DEAR

around the cylindrical target, in order to reach a high transmission efficiency of the soft X-rays.

In fig. 2.2 the main components of the set-up are indicated: the beryllium cylindrical window, through which the K^-s, produced by the ϕ decays, leave the DAΦNE pipe; the vacuum box, containing the cylindrical target cell, with cooled and pressurized hydrogen inside, and outside the CCDs.

The selection of the hydrogen density has been optimized taking into consideration the number of stopped kaons, the eventual decrease of the X-ray yield due to Stark mixing with an increase in density, the K^- life time (which is a relevant parameter due to the K^- low momentum), and the thicknesses of different windows interposed through the K^- path. The optimum choice is a hydrogen pressure 3 atm and a temperature 25 K, obtained using a liquid helium cryogenic system. The resulting target density is $3.6 \cdot 10^{-3} g/cm^3$. As described in Chapter 5, the expected yield of K_α X-rays per stopped kaon in these conditions turns out to be about 3%.

Having fixed the target density, the overall dimensions of the set-up together with the window thicknesses were determined using the Monte Carlo simulation code described in Chapter 6.

In fig. 2.3, the front view of the set-up is shown. The beam pipe has a radius of 5.3 cm and the beryllium cylindrical window a thickness of 400 μm and a length of 15 cm. Just outside the beryllium pipe and all around it, a 2.1 mm thick cylindrical plastic degrader is placed, not only with the aim of slowing down the K^-s, but also to protect the beryllium pipe.

Moving upward, along the positive y-axis, we find, after 2.5 cm of air above the degrader, the vacuum box, made of Al, 1.5 cm thick and 24 cm size square. Kaons enter the vacuum box through a circular Al window, 10 cm diameter and 400 μm thickness. A second coaxial Al window, 11.5 cm diameter and 100 μm thick, is placed 1.5 cm above, as a heat shield. After 4.5 cm of vacuum, there is the 400 μm thick beryllium window of the cylindrical target cell, whose axis coincides with the y-axis. The cell diameter is 15 cm and its height is 12 cm. The lateral and top walls of the cell are made of Al, 3 mm thick.

The CCD detectors are arranged in 4 couples, each couple at 90° with respect to the contiguous one, all around the lateral wall of the cylindrical target cell, for a total number of 8 CCDs. Each CCD, whose dimensions are 2.7 cm height and 1.7 cm width, is put vertically, and each couple is formed with the two CCDs one above the other, separated by 8 mm. The distance from the bottom of the target cell to the center of each CCD pair is 8 cm, and corresponds to the mean position of the stopped K^-s, in order to maximize the acceptance for the emitted X-rays. In correspondence to the position of each CCD pair, there is an equal number of windows made of Kapton, 25 μm thick.

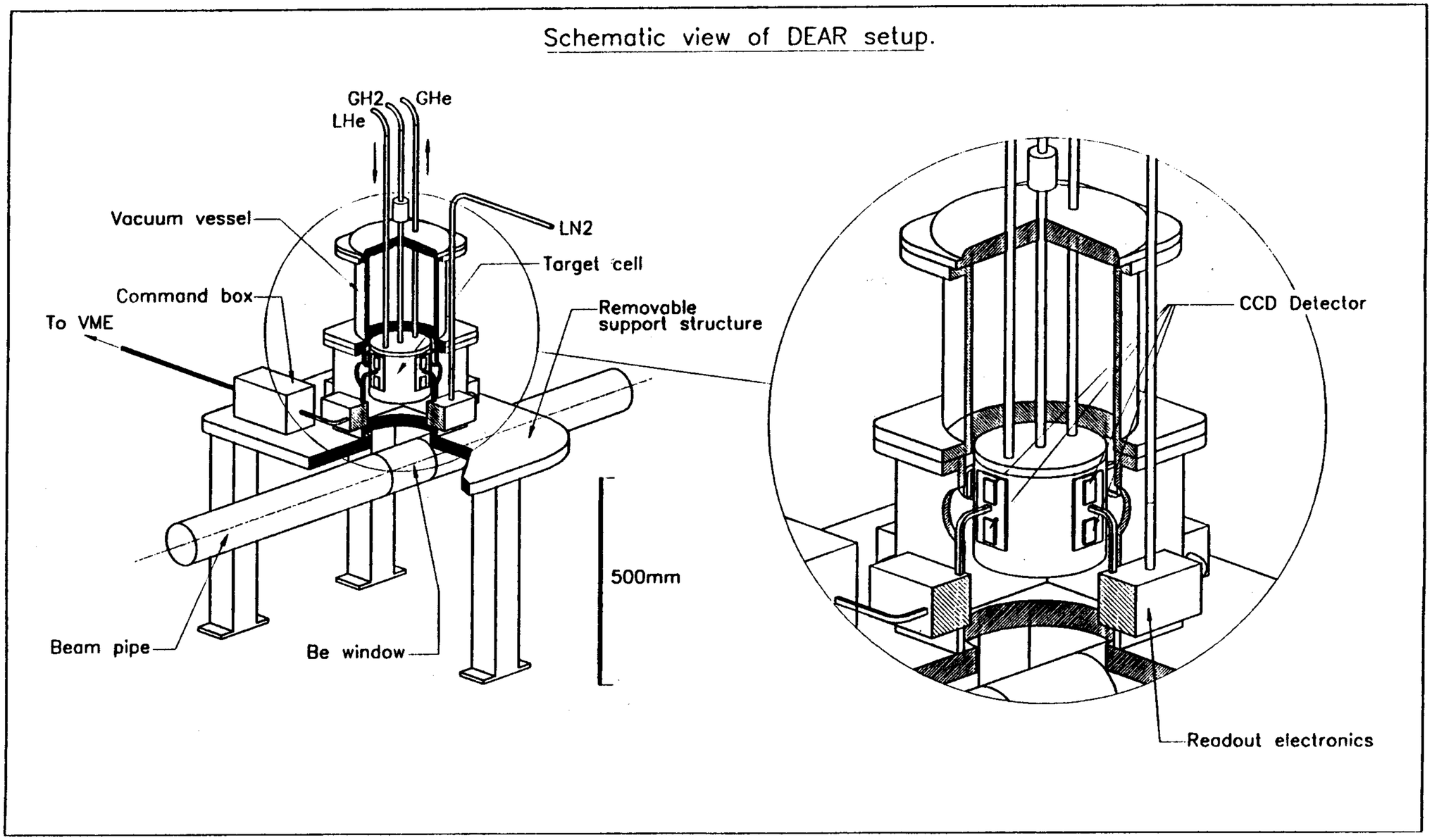

Figure 2.2: Schematic view of the DEAR experimental set-up

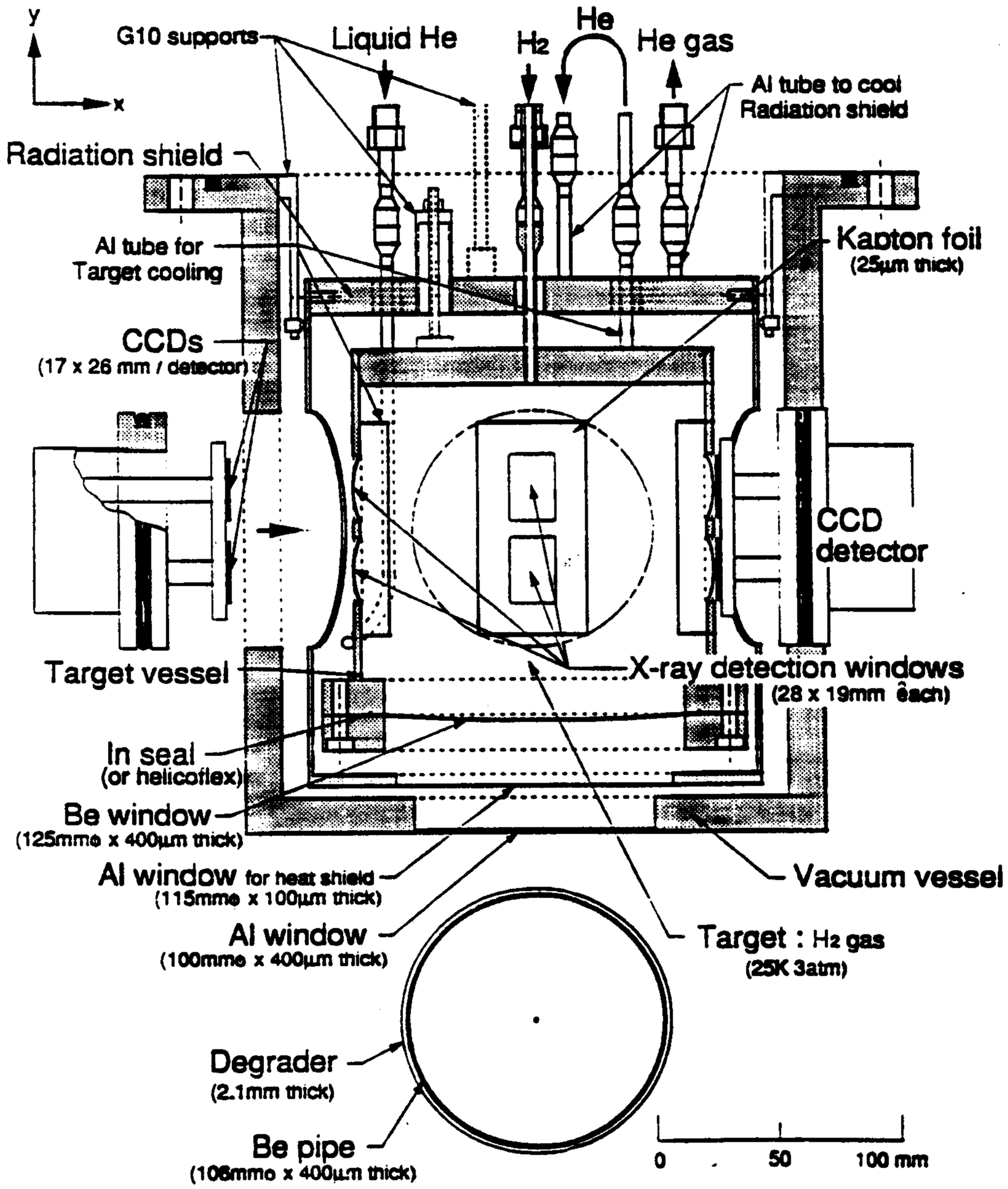

Figure 2.3: Front view of the DEAR experimental set-up, showing the detail of the pipe and target region.

In each of the four lateral surfaces of the Al vacuum box, corresponding to the position of each couple of CCDs, a hole of 10 cm diameter is made, in order to allow the insertion and removal of the CCDs, the passing of cables and of the cold finger (cooled by liquid nitrogen) and the readout electronics to operate the CCD. Above the top wall of the Al box is the cryogenics system of the target, described in Chapter 4.

Chapter 3

CCDs (Charge-Coupled Devices)

3.1 Introduction

The CCD concept [1] was proposed in 1970 by Boyle and Smith [2]. The essential feature of their scheme was to store information in the form of electrical charge packets in potential wells which were created in a semiconductor by the influence of overlying electrodes separated from the semiconductor by a thin insulation layer. The potential wells and therefore the charge packets could be shifted through the semiconductor by applying voltages (phases) to the electrodes, providing a readout. It was soon realized that charges could be introduced into the potential wells by optical means. It was therefore possible to collect and read out the charges created by incident light and the CCD as an image sensor was born. Already in 1974 a 320 $\times$ 512 pixels CCD sensor for television was demonstrated [3].

CCDs are solid state detectors with a pixel structure [1], [4], (fig. 3.1). The separation of the columns is done with a channel stop (NPN diode structure) between each column. The rows are separated by potential wells which are produced by an array of electrodes mounted on top of the depletion layer. Three electrodes are needed for one pixel. When a CCD is in accumulation mode, a positive voltage is applied to two of them and a negative voltage to the third. For the readout, the accumulated electrons are shifted to a special readout line at the end of the columns, electrode by electrode, by applying three AC voltages with the proper phases to the electrodes of the pixels.

Although CCDs were initially developed for detecting light and mainly to be used in video cameras, they are also very good X-ray detectors in the energy range from 1 keV (limited by the thickness of the electrodes) to 12 KeV (limited by the depletion depth). This leads to applications in X-ray spectrometry, as here in this proposal, or in X-ray astronomy. More generally, sophisticated X-ray versus particle discrimination might also prove useful in future X-ray satellite missions with CCD detectors, since X-rays will have to be cleanly separated from all other cosmic rays [5]. A different application is the position measurement of charged particle tracks.

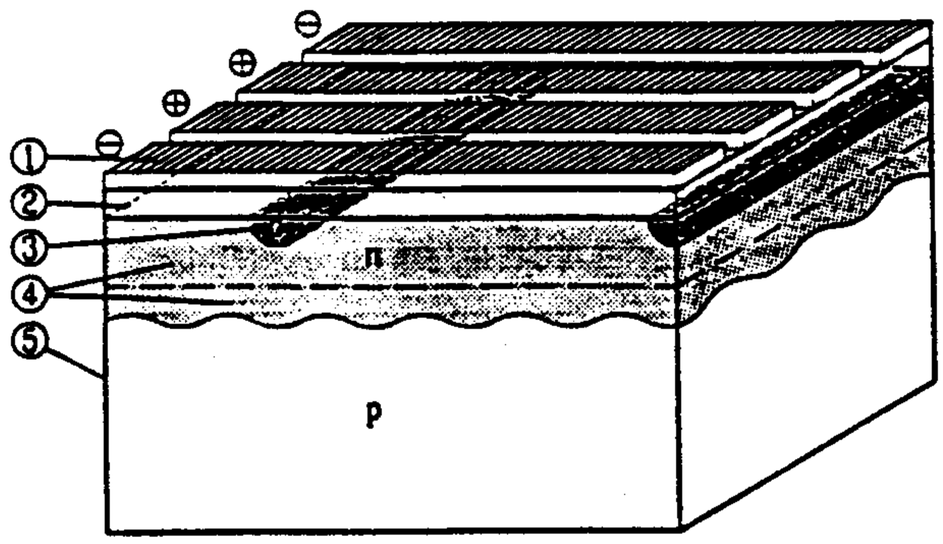

Figure 3.1: Pixel structure of a CCD: (1) electrodes, (2) insulator, (3) channel stop, (4) depletion layer and (5) p- and n- silicon.

However, for high energy physics applications the CCDs are usually too slow; silicon strip detectors are used instead [4].

The good two dimensional spatial resolution of the CCDs (22.5 μm $\times$ 22.5 μm) turns out to be crucial to extract the weak signal out of the large background, which is one of the characteristics of the kaonic hydrogen experiments. In most cases X-rays produce single-pixel events, whereas the tracks of charged particles produce cluster events with more than one hit pixel (see fig. 3.2). The usual way to distinguish X-rays from background (mainly charged particles and higher energy gamma rays) is to require that none of the 8 surrounding pixels have a charge that is considerably above the noise level. If all eight surrounding pixels are below this limit, the event is considered an X-ray. A total background discrimination (except for X-ray background) can be achieved by applying other tests, e.g. on the mean value or on the standard deviation of the energy of the eight neighboring pixels [6].

The CCDs we use [7] are MOS type made of silicon. The low Z of Si reduces the detection efficiency above a few KeV. In addition, Si has an absorption edge at 1.84 KeV, resulting in large detector efficiency variations. A more constant detector efficiency as a function of soft X-ray energy can be obtained with germanium CCDs (the Ge K absorption edge is at 11.1 KeV). In addition, Ge is a better semiconductor for X-ray detection above 10 keV because of its higher Z value. However, the Ge oxide needed for the CCD surface (MOS type) does not have sufficient resistivity. A new development based on GaAs technology would probably work, but has not yet started. New Si p-n CCDs exist, but their pixel size is too large at the moment.

Work started on X-ray detection with CCDs in Neuchâtel in 1986 and a first prototype system was working in 1988. Since then the reliability, the energy resolu-

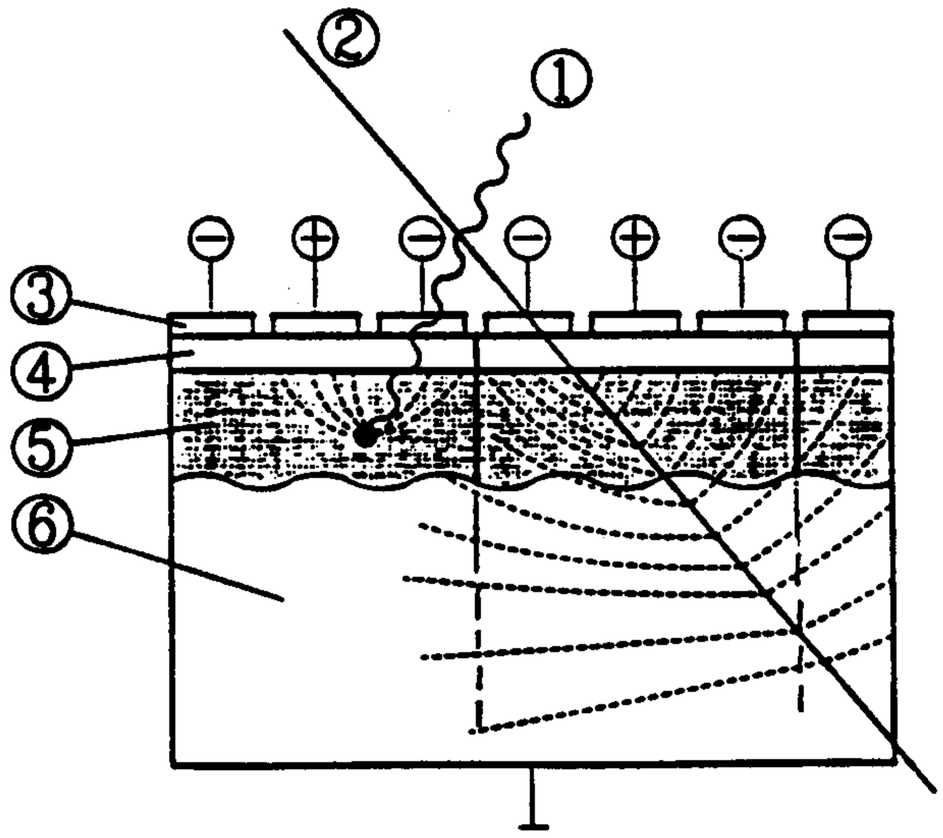

Figure 3.2: Particle detection in a CCD: (1)X-ray, (2)charged particle track, (3)electrodes, (4)insulator, (5)depletion layer and (6) bulk material. A pixel covers 3 electrodes. The depletion layer is 6 μm for normal CCDs and 30 μm for deep depleted CCDs. All our CCDs are deep depleted. The bulk material is approximately 1 mm thick. The dotted lines correspond to possible e^- migration.

tion and especially the background suppression of the CCD systems were improved. In addition, the detection surface was increased approximately 20 times. Collaborations were formed to measure pionic and muonic X-rays at PSI (Paul Scherrer Institute, Villigen) and antiprotonic hydrogen X-rays at CERN (LEAR). References on the work in Neuchâtel (some of which are already partially obsolete), are given in [8].

3.2 Performance

3.2.1 Measured energy resolution (in beam)

In beam measured energy resolution (FWHM) is given in the table below:

X-ray energy $[KeV]$	energy resolution (FWHM) $[eV]$
2	$\leq$ 120
3	140 - 150
6	$\approx$ 170
8	$\approx$ 190

The energy resolution depends slightly on the CCD exposure time. The resolution values are better than those of other comparable detectors.

The energy resolution of a CCD is given by:

$$\Delta E\,(FWHM) \;=\; 2.355 \times \omega(N^2 + \frac{FE}{\omega})^{1/2}\,(eV)$$

with

E = X-ray energy

F = Fano factor $\approx$ 0.12

ω = conversion energy for an electron-hole pair in Si = 3.68 eV

2.355 = r.m.s. $\rightarrow$ FWHM conversion factor

N = r.m.s. transfer and readout noise.

As an example, the number of electron - hole pairs created by a 6 KeV X-ray is 6 KeV/3.68 eV which is about 1600.

From the preceeding formula, N can be calculated. It varies between 10 and 15 electrons r.m.s. in our case. These are realistic, in beam values. Work in Neuchâtel has concentrated on reducing N as much as possible, but N is now dominated by the noise of the on-chip amplifier. Further noise reduction can be obtained by reading a pixel several times over and averaging. However, the readout time becomes prohibitive (see paragraph 3.2.4). By putting N = 0, the theoretically best possible energy resolution can be calculated. It corresponds to $\approx$ 70 eV FWHM at 2 KeV and $\approx$ 140 eV FWHM at 8 KeV.

3.2.2 Background rejection

The CCD background rejection capabilities are very powerful, even though our CCDs cannot be triggered. In fact CCDs have a much better signal/background ratio than Si(Li) detectors, which are triggered (see figs. 3.3 and 3.4). This may be somewhat surprising. One has to keep in mind that in the environment of an accelerator a lot of the background is event correlated and triggering is therefore less effective. With CCDs, however, background (except soft X-rays) can be completely eliminated. As said in the introduction, this is based on the fact that, in most cases, an X-ray in the 1 - 10 KeV energy region deposits its energy in a single pixel of 22.5 μm $\times$ 22.5 μm. Charged particles, gammas and neutrons, on the other hand, are split into several pixels. Background, for example at the πE5 beam line at PSI, fills, on the average, 5.5 pixels and the most probable hit is 4 pixels. Since a pixel has 8 neighbors, **a good X-ray event is a single pixel hit surrounded by 8 pixels which are part of the noise.** In a very high background environment, the 8 pixels surrounding an X-ray event have to be examined statistically to make sure that they are part of the noise peak [6]. The intrinsic CCD noise is $\approx$ 200 eV.

Why does a soft X-ray hit mostly only 1 pixel and charged particles hit several? The interactions are different. Soft X-ray interaction is by photoelectric effect which is localized in space within the depletion layer, whereas charged particles loose energy by ionization everywhere in the silicon (see fig. 3.2). The electrons of the electron - hole pairs created in the silicon cannot escape if they are in the potential well of the depletion zone of the pixel. However, in the border regions of a pixel, and especially in the bulk material, these electrons can move almost freely. This movement is enhanced by a suitable voltage applied to the bulk. Since, for topological reasons, all charged particles will at some time cross pixel borders, they can be eliminated. Of course some X-rays in the border regions will also be eliminated, but, by chance, the pixel size is just right for a good soft X-ray detection efficiency, as needed in the kaonic hydrogen experiment.

Soft X-ray background, however, cannot be eliminated. As can be seen from figs. 3.3 to 3.5, the contributions from stainless steel (e^-Fe, K_α: 6.40 KeV, K_β: 7.06 KeV and e^-Cr, K_α:5.41 KeV, K_β:5.95 KeV) are important and in the vicinity of the kaonic hydrogen K-series signal. The target and the CCD detection system should therefore be made, when possible, of other materials (Al for example) or be painted with TiO_2 paint (e^-Ti, K_α: 4.5 KeV).This energy is well separated from the expected kaonic hydrogen X-ray energies (see 3.2.6) and may also be used as a calibration line.

3.2.3 Examples of measured X-ray spectra at PSI and CERN

Examples of measured X-ray spectra in muonic deuterium, pionic and antiprotonic hydrogen are presented in figs. 3.3 - 3.5.

Muonic hydrogen, deuterium and helium X-rays are measured at PSI in 2 collaborations:

- QED test in muonic hydrogen with a free electron laser (E. Zavattini)
- Muonic hydrogen to helium transfer; knowledge of the muon-catalyzed fusion cycle (W. Breunlich and J.-P. Egger).

Pionic hydrogen and deuterium X-rays have been extensively measured at PSI, mainly with a high resolution crystal spectrometer (A. Badertscher and J.-P. Egger). These experiments are finished and are being published. The strong interaction parameters (shift and width) have been determined very precisely. In particular, the pionic hydrogen $1s$ strong interaction shift was determined with a precision of $\pm$ 0.04 eV. For comparison, the precision we hope to obtain according to this proposal for the kaonic hydrogen $1s$ strong interaction shift is $\leq$ 10 eV.

Antiprotonic hydrogen is being measured at CERN (LEAR, PS 207).

The quality of the CCD spectra of figs. 3.3 - 3.5 speaks for itself.

3.2.4 CCD size and readout time

The number of pixels per CCD is 770 × 1152 ≈ 887000. The CCD surface is ≈ 17 × 26 mm^2 ≈ 4.5 cm^2. The two halfs of each CCD are read out simultaneously. Today, up to four CCDs can be read out at the same time. This will be increased to the 8 CCDs necessary for the experiment. The transfer and readout time per pixel is 64 μs. The total readout time of the system (= 1/2 CCD readout time) is 64 μs × 444000 ≈ 28 s. Accumulation of data continues during the readout. The pixel readout time could be reduced to 20 μs at the expense of a 30 % loss in energy resolution, according to recent measurements performed at Neuchâtel.

The CCD collection time should not be too long, so that the same 8 pixel cluster which defines a good X-ray event is not hit twice. To be safe, *the number of hit pixels should not exceed ≈ 5 %, corresponding to approximately 4000 - 5000 background events per 1/2 CCD.* Based on Monte-Carlo calculations presented in Chapter 6, the safety limit on DAΦNE is reached after 50 min of data taking. Taking a factor of safety of 10, the CCD exposure time at DAΦNE can be of 5 min, which is very comfortable.

3.2.5 CCD detector efficiency

The total X-ray detection efficiency is a product of the intrinsic CCD efficiency, and the X-ray transmission through the different windows and through the hydrogen gas in the target. The CCD efficiency is given in fig.3.6.

3.2.6 Expected kaonic hydrogen X-ray energies

The X-ray energies to be detected are reported below (no strong interaction shift included in the K-series). The CCDs are ideal detectors in this energy range.

	K_α	K_β	K_∞	L_α	L_β	L_∞
kaonic hydrogen $[KeV]$	6.46	7.66	8.62	1.20	1.62	2.15
kaonic deuterium $[KeV]$	7.81	9.25	10.41	1.44	1.95	2.60

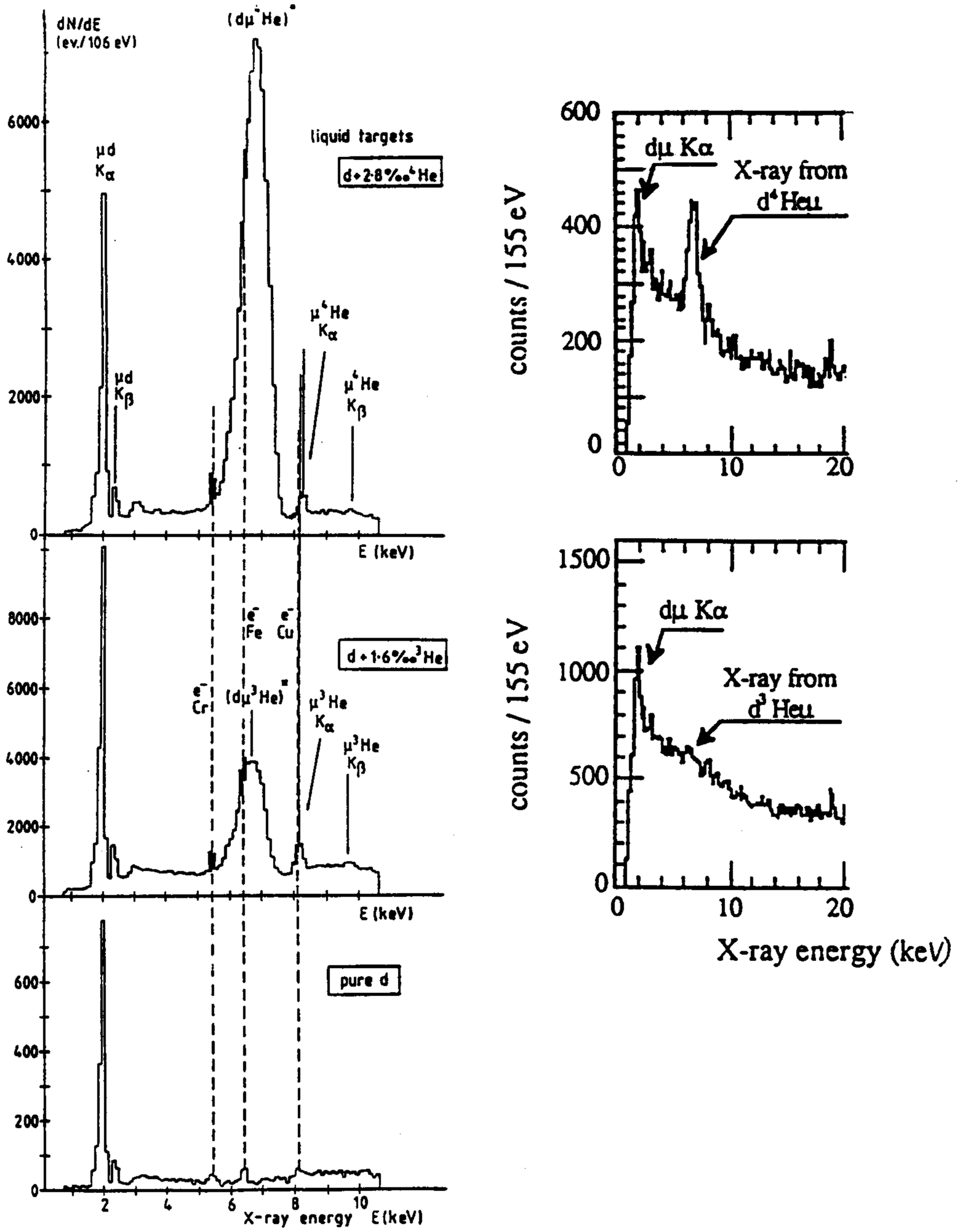

Figure 3.3: Muonic deuterium energy spectra taken at PSI at the μE4 channel with two 4.5 cm^2 CCDs [9]. The target is a liquid target, either pure or with small admixtures of 3He or 4He. The energy resolution is sufficient to separate the muonic deuterium K_α and K_β lines. When the helium is present, the muon forms a molecular state that emits a 6.8 KeV X-ray. This muon transfer mechanism is part of the muon-cathalyzed fusion cycle. Some X-ray contaminants from the stainless steel and copper target vessel are shown in black. On the right the same spectra taken at KEK [10] with Si(Li) detectors are shown.

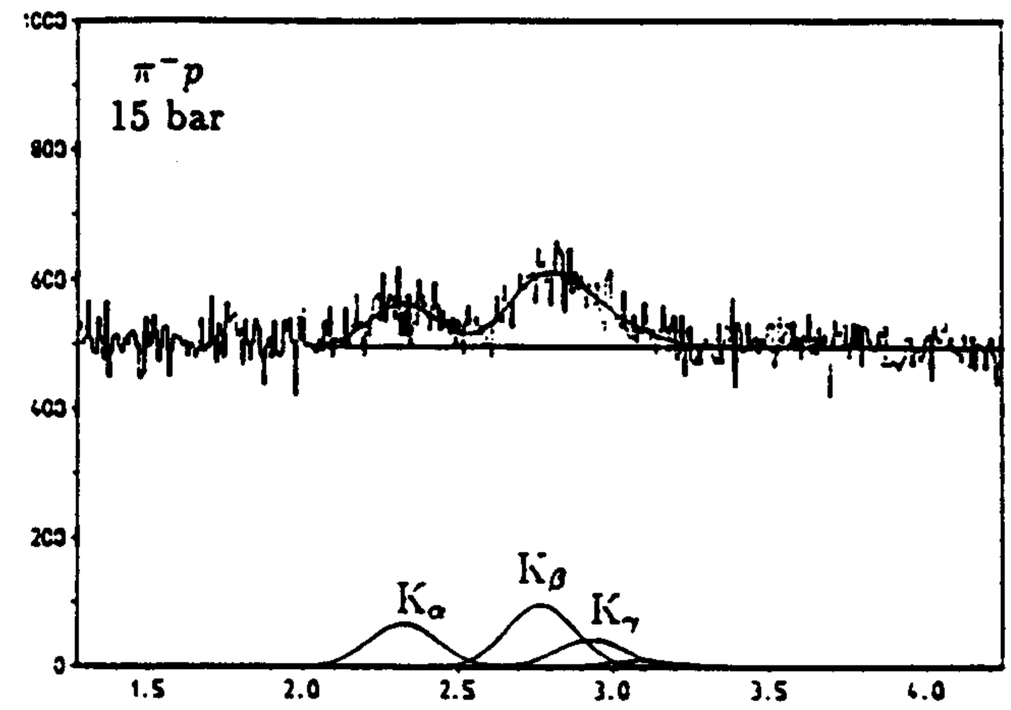

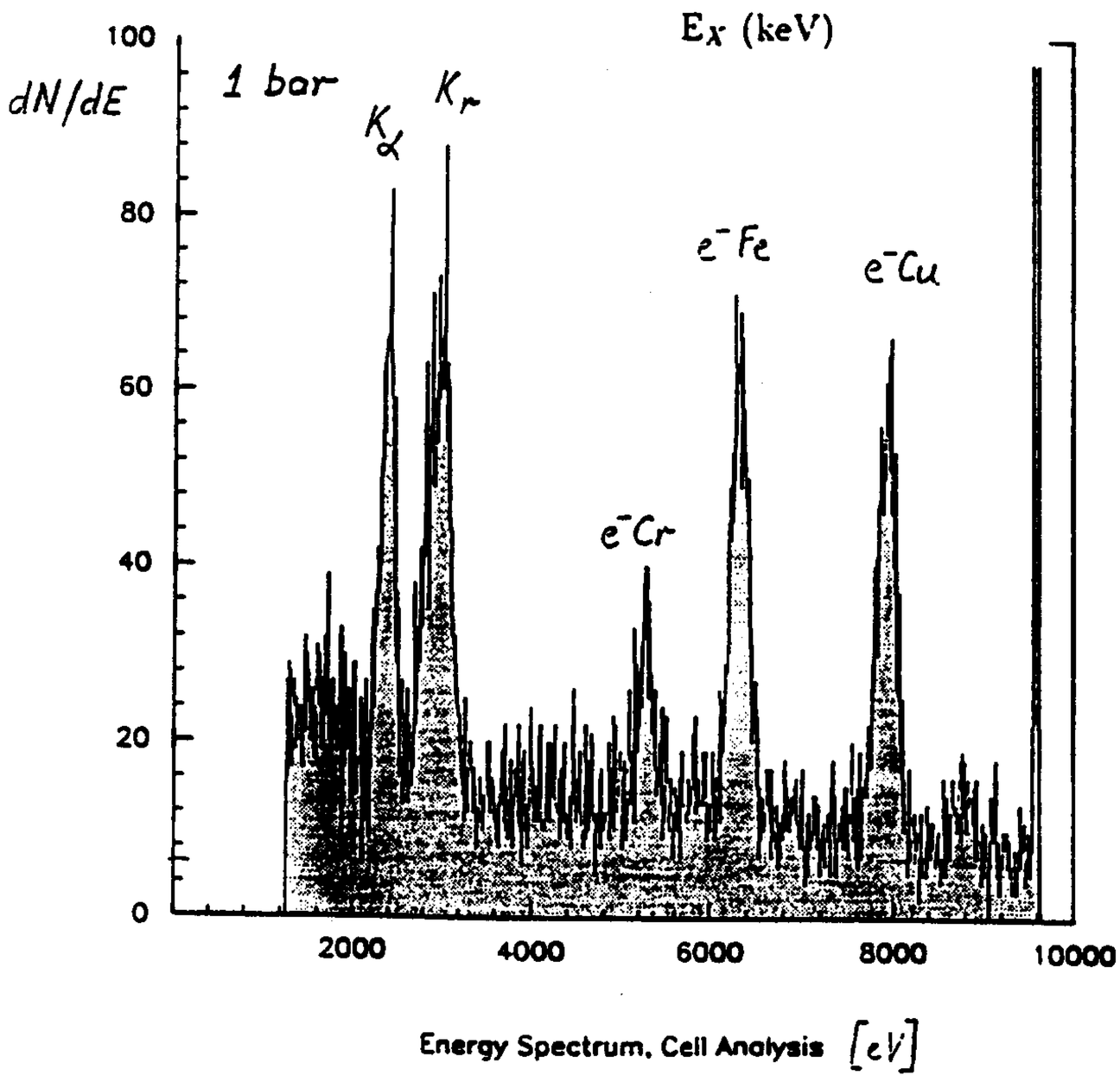

Figure 3.4: (bottom): Pionic hydrogen energy spectrum taken with an 1 cm^2 CCD. The target was a simple 1 atm gas target at normal temperature. These data were taken in the high background environment of the πE5 channel at PSI (10^8 π^-/s of 85 MeV/c, $3 \cdot 10^8$ e^-/s, cyclotron trap). The pionic hydrogen K_α yield (E=2.44 KeV) is approximately 8–9%, which is similar to the estimated kaonic hydrogen yields. CCD exposure time was 1 min and total measurement time 12 h. (top): Pionic hydrogen energy spectrum taken at PSI under similar experimental conditions with a Si(Li) counter of 0.5 cm^2 [11]. In order to see a signal the target density was increased 15 times with respect to the CCD spectrum conditions.

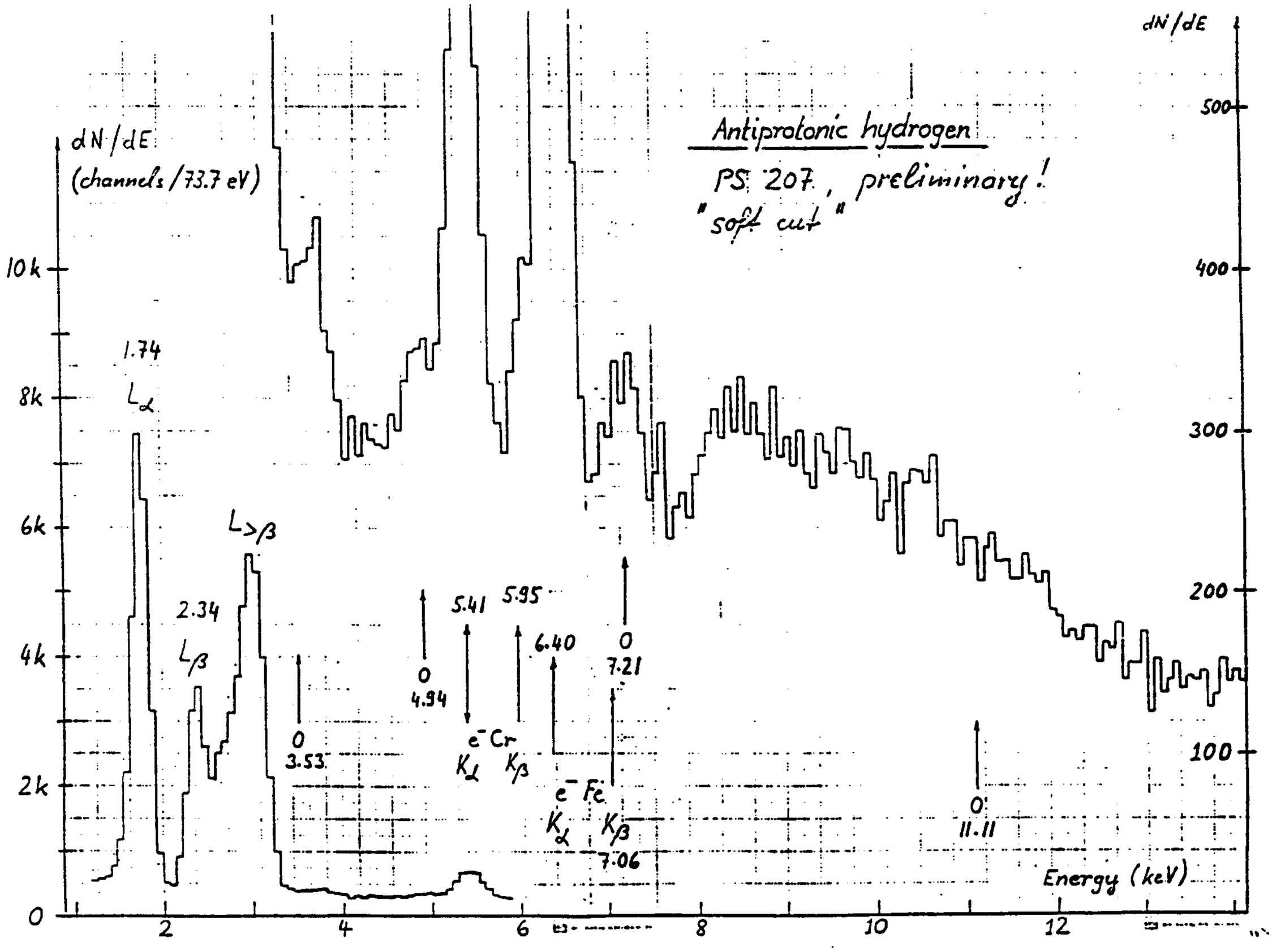

Figure 3.5: Preliminary antiprotonic hydrogen spectrum taken during the 1994 PS207 run at LEAR (CERN) with a gas target at a pressure of 30 mbar. 105 MeV/c antiprotons and the cyclotron trap were used. A 1 cm^2 CCD was read out every 8 s and over 1000 files were added.

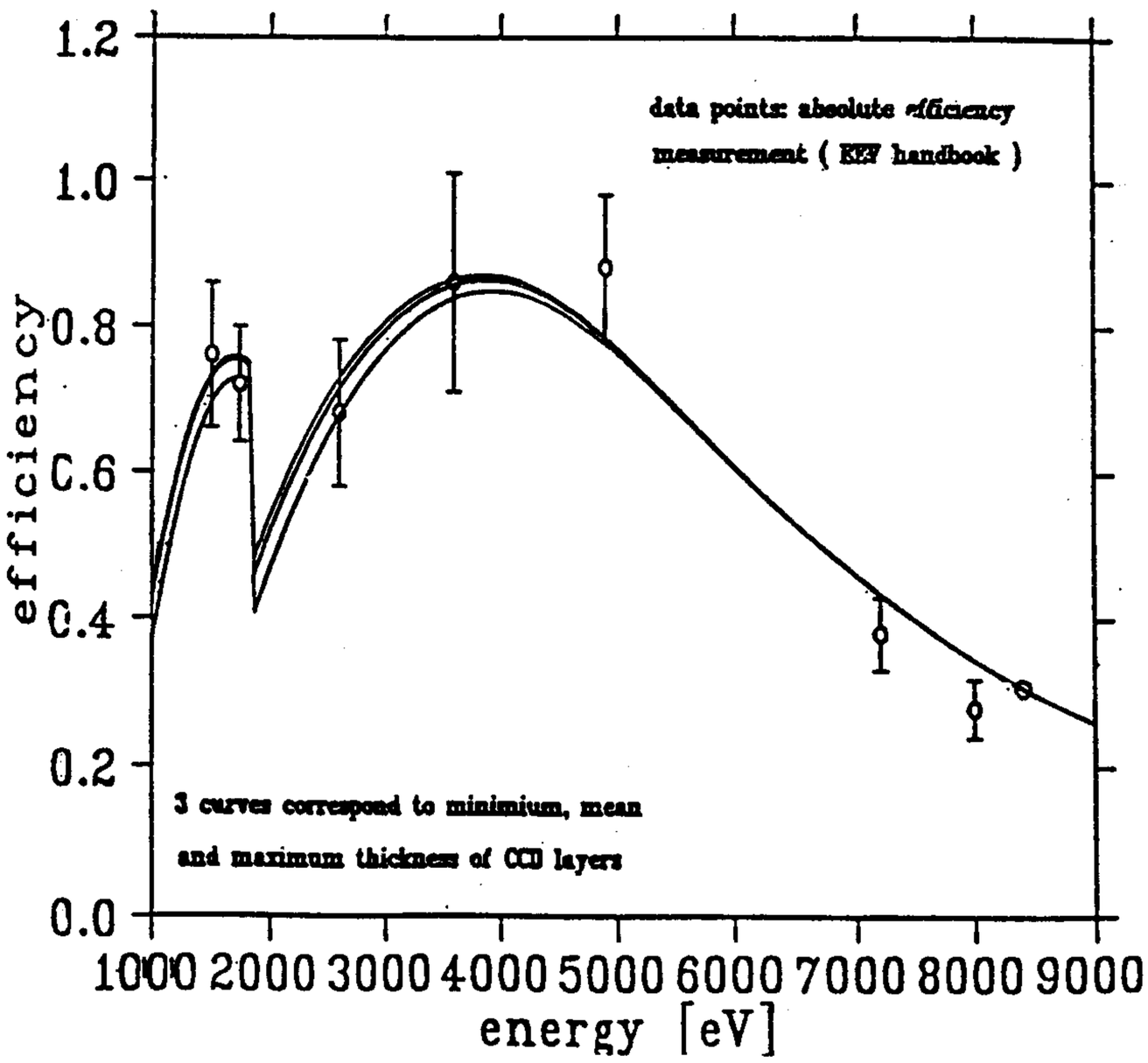

Figure 3.6: Absolute CCD efficiency without any window. The Si absorbtion edge at 1.84 KeV is clearly seen.

3.3 Set-up

3.3.1 Block diagram

The block diagram of the CCD set–up is shown in fig.3.7. Normally the CCDs are operated from a PC. In local mode, the CCDs can also be run from the command box. This is useful for trouble shooting.

3.3.2 Temperature, vacuum, etc.

The CCDs are kept at a temperature between -95°C and -120°C during a run. The temperature is measured at some points between the CCDs and the liquid nitrogen container with PT100 monitors. A feedback system allows for stabilizing the CCD temperature at a preset value with a small heater. The CCD temperature is displayed at the command box. The CCDs need to be in vacuum. This vacuum is usually of the order of 10^{-6} mbar, although 10^{-3} mbar would be sufficient. It is possible to put the CCDs inside the insulation vacuum of a cryogenic target. It is also possible to run them in a strong magnetic field.

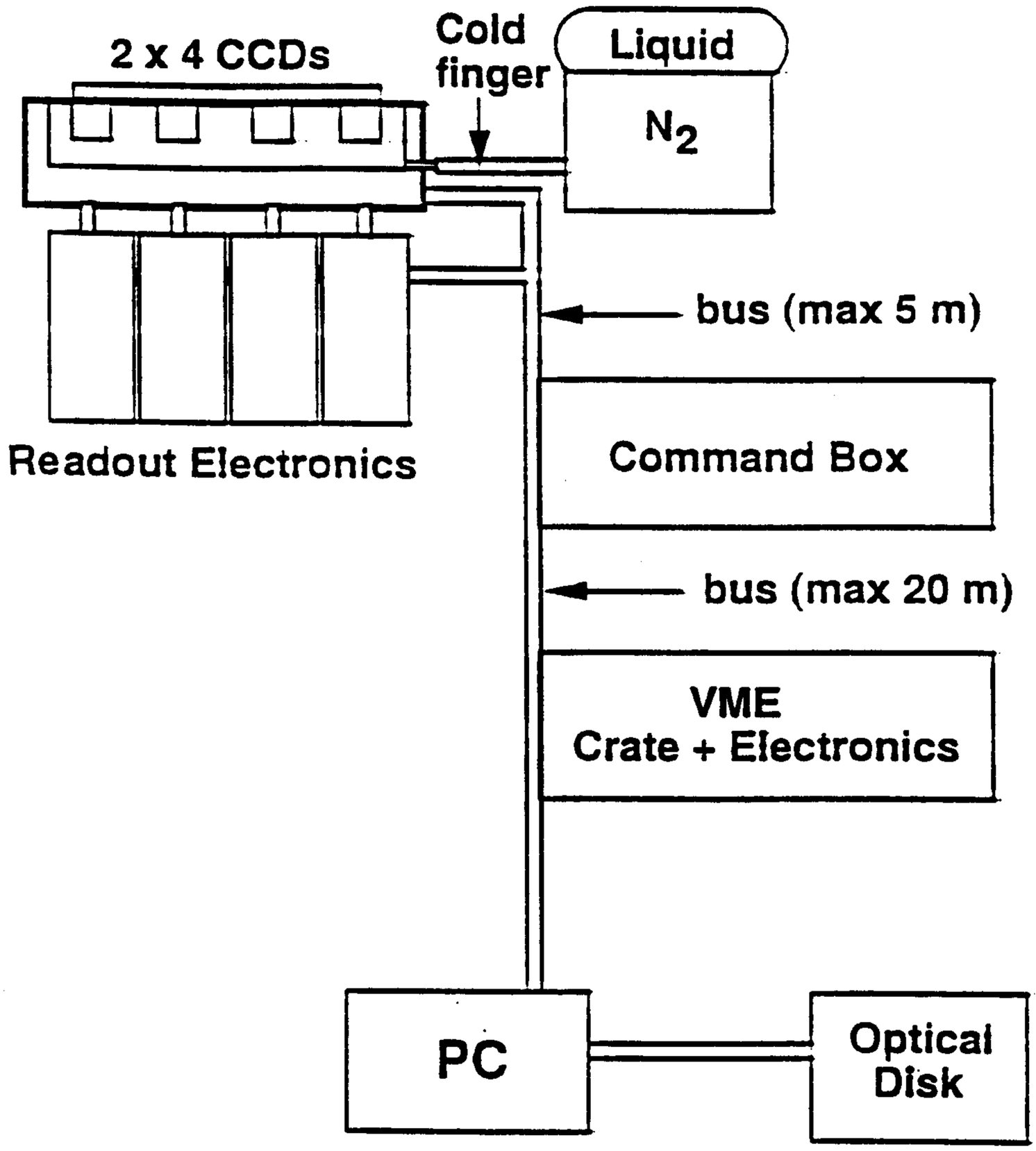

Figure 3.7: Block diagram of the CCD X-ray detection system.

3.3.3 Readout electronics

The readout electronics was optimized for low noise. Of the various possibilities that exist to read the analog signal of CCDs, the *correlated double sampling* technique reaches the lowest noise level, and was therefore chosen. Since the reset noise is constant during one charge transfer, it is sampled twice, subtracted from the signal and can therefore be eliminated. The remaining dominant noise is the output amplifier noise.

3.3.4 Command box

This box generates the logic signals and command signals and is a power supply for the phases (voltages by which the charges are transferred), CCDs, readout circuit and ADC.

3.3.5 VME electronics and computer

The VME crate contains a BIT-3 crate controller and a CCD control module with a 2 Mbyte 32-bit memory buffer. During the readout cycle the CCD data are written into this buffer and then transferred to the PC with a large hard disk, 32 Mbyte memory and a 1.3 Gbyte magneto–optic disk for data storage.

3.4 Data acquisition and on-line analysis

Since there are no triggers, fast coincidences, interrupts, etc., data acquisition is very simple. Events are collected into the CCDs for a finite time and are then read out. The long exposure time which is possible with the kaonic hydrogen experiment (see paragraph 3.2.4) allows for a full on-line analysis.

The data acquisition and on-line analysis software run under Microsoft WINDOWS. Data acquisition can be preset and is then automatic. When no command is given, the CCDs are always in accumulation mode, taking data. There are only two CCD commands: CLEAR and READ + CLEAR. After a READ + CLEAR command the CCD matrices are stored on the magneto–optic disk. Between readouts on-line analysis can be carried out with different programs. A VIEW program displays the CCD matrices and calculates the single, double, triple etc. hits. A PREANALYSIS program fits the CCD noise peak, takes its center as zero energy (calibration), throws the noise peak away and does a soft single pixel cut. The events that passed the test are stored in a small file on magneto–optic disk. The ANALYSIS program allows for statistical cuts and displays energy, position, hit pixel and all other possible parameters. In addition, fits can be made to determine position and width of peaks. The VIEW and PREANALYSIS programs take about 10 s each and can be included in the automatic data taking if data taking time permits. The

analysis program takes a few minutes.

It is therefore possible, for example, to see and print out a kaonic hydrogen X-ray energy spectrum with sophisticated background cuts, any time during the experiment.

3.5 Calibration

The primary calibration and performance monitor of the CCD detectors will be, when beam is on, the electronic K_α and K_β X-rays from the ionization of titanium atom at 4.5 and 4.9 KeV, respectively. As at KEK, a thin Ti foil will be placed at the target exit window to produce these lines. Additionally, conventional X-ray sources such as ^{55}Fe (Mn, K_α: 5.89 KeV, K_β: 6.49 KeV) and ^{57}Co (Co, K_α: 6.93 KeV, K_β: 7.65 KeV) can be viewed through the entrance window to provide an off-line calibration. The stability of these detectors is exceptional, with no significant change observed in the same detector over a series of $\pi^- p$ and $\bar{p}p$ measurements.

Bibliography

[1] J.D.E. Beynon and D.R. Lamb, *Charge-coupled devices and their applications,* Mc-Graw Hill (London) 1980.

[2] W.S. Boyle and G.E. Smith, *Charge-coupled semiconductor device*, Bell Syst. Tech. Journal **49** (1970) 587.

[3] R.L. Rodgers, *Charge-coupled imager for 525-line television*, Digest of IEEE Intercon, March 1974, Session 2.

[4] G. Charpak and F. Sauli, Ann. Rev. Nucl. Part. Sci. **34** (1984) 285.

[5] J.L. Culhane, Nucl. Instr. and Meth. **A310** (1991) 1.

[6] D. Sigg, Nucl. Instr. and Meth. **A345** (1994) 107.

[7] EEV (English Electric Valve), Waterhouse Lane, Chelmsford, Essex, CM1 2QU, England.

[8] J.-P. Egger, D. Chatellard and E. Jeannet, *Progress in soft X-ray detection: The case of exotic hydrogen*, Particle World **3** (1993) 139;
G. Fiorucci *et al.*, Nucl. Instr. and Meth. **A 292** (1990) 141;
D. Varidel *et al.*, Nucl. Instr. and Meth. **A 292** (1990) 147.

[9] B. Gartner, thesis, Austrian Academy of Sciences, Vienna.

[10] T. Matsuzaki *et al.*, Muon Cat. Fusion **2** (1988) 217;
Y. Watanabe *et al.*, Muon Cat. Fusion **5/6** (1990/91) 93.

[11] A.J. Rusi El Hassani *et al.*, Z. für Physik **A351** (1995) 113.

Chapter 4

The DEAR cryogenic gaseous target

4.1 The target set-up

To achieve high stopping density of the kaons in front of CCD detectors without decreasing X-ray yield due to Stark mixing effects, we have studied a gaseous pressurized cryogenic target. Let's summarize the requirements to the target system.

- The target should be operated at 25K and 3 atmospheres.
- Only low Z materials can be used around the target.
- The multiple scattering of kaons should be minimum.
- It should be designed in such a way that an accurate positioning of the target is possible to maximize the solid angle seen by the CCD detectors.
- It should have 4 entrance windows for CCD detectors.
- To reduce the helium consumption, it must be equipped with a radiation shield.
- Time stability is important and moreover it must be well constructed for safety.

To satisfy these requirements, we have designed the cryostat system shown in fig. 4.1 and 2.3, and the gas flow diagram shown in fig. 4.2. The lower part of the cryostat is square-shaped to fit the CCD detector system and the four entrance windows open on each side. All the materials of the lower part of the cryostat are made of aluminum, except some windows and glass reinforced plastic supports (G10 supports). Most commonly used materials for cryogenic systems are iron (stainless steel : SUS) and copper. However, these materials cannot be used in our case due to their characteristic X-ray sitting in the energy region of interest. We will machine out the kaon entrance window of the vacuum vessel (100 mmϕ $\times$ 400μm thickness)

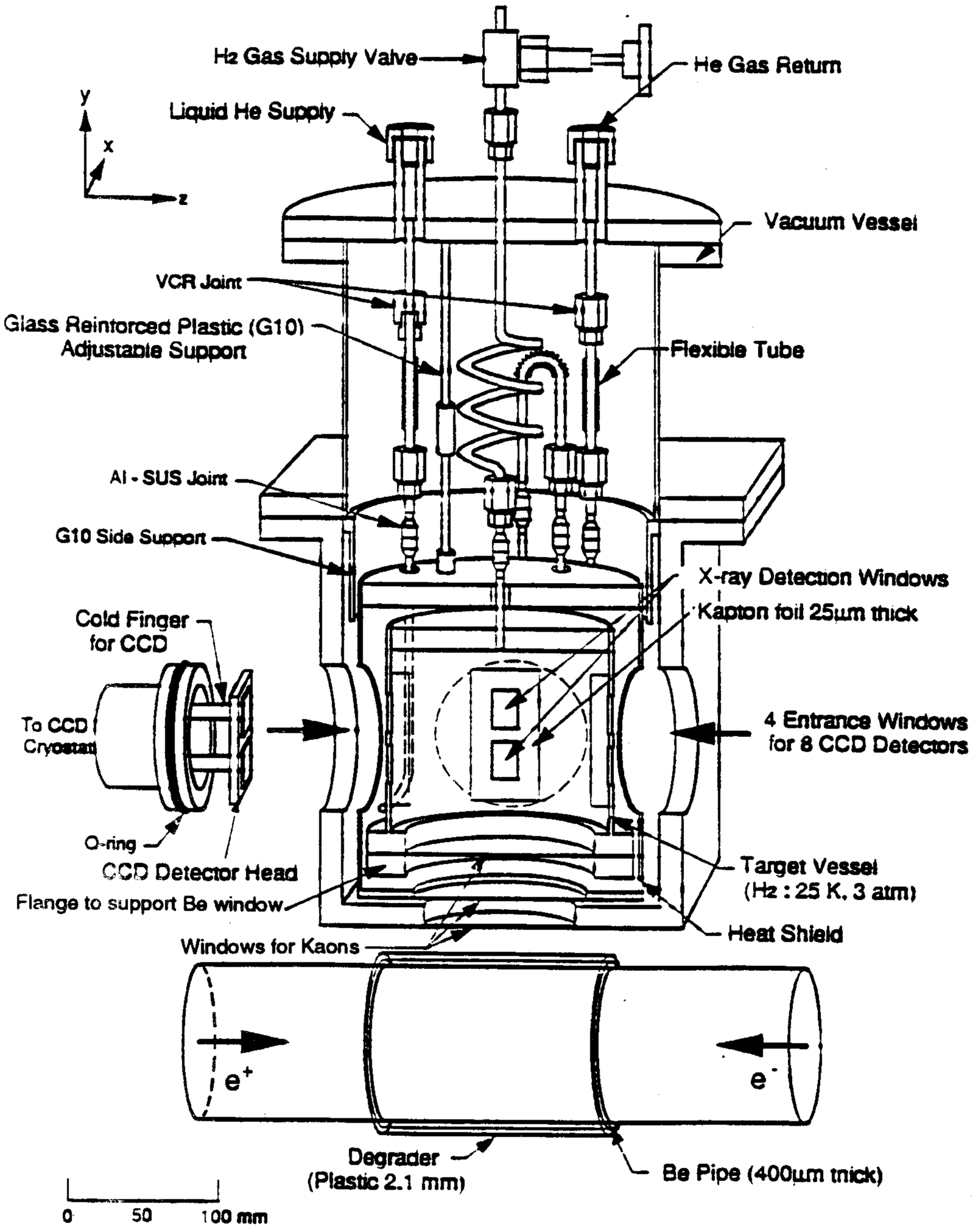

Figure 4.1: The DEAR cryostat system

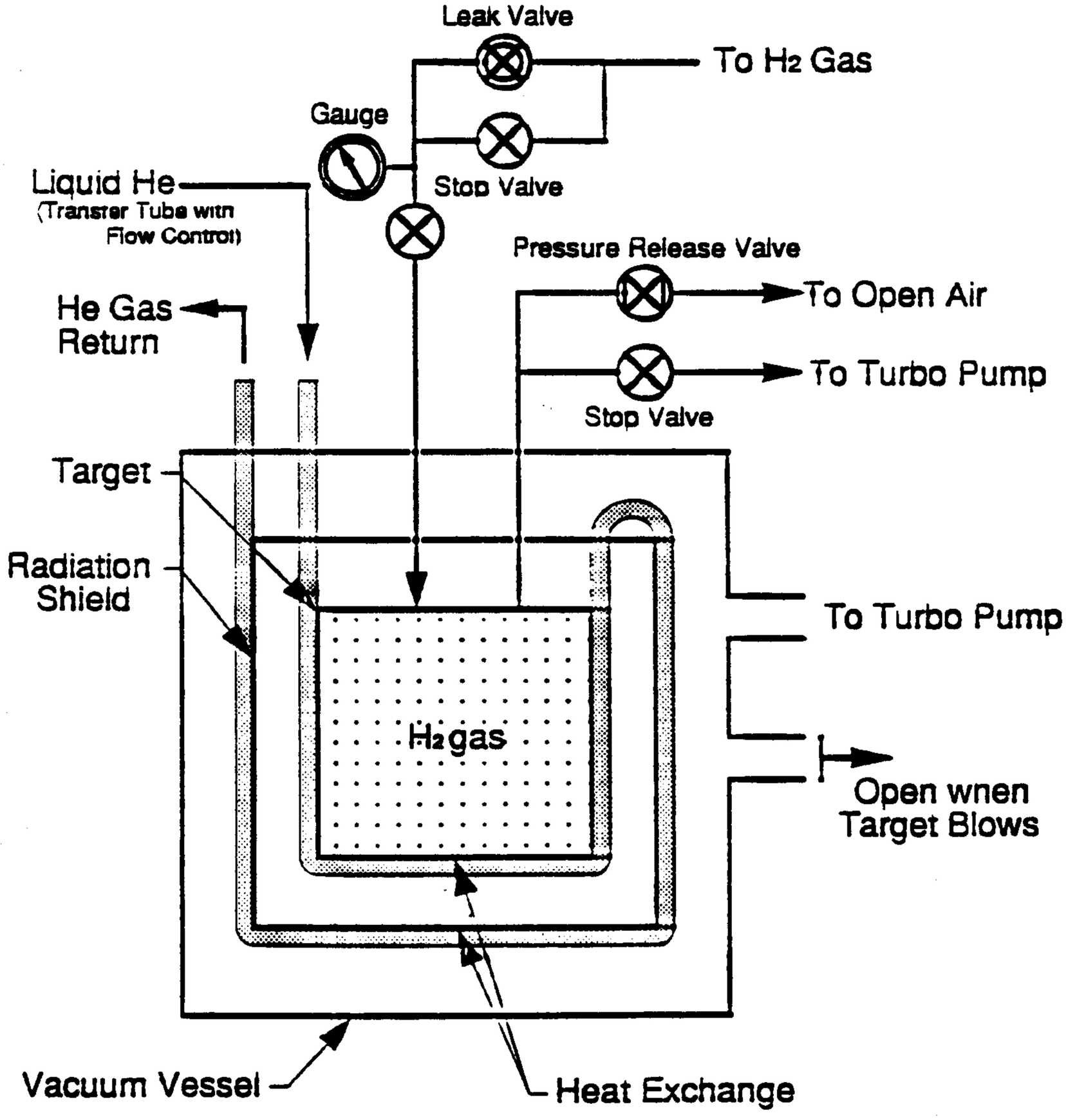

Figure 4.2: The target gas flow diagram

from an aluminum block, in order to get enough strength in the direction of the beam pipe.

The size of the target vessel is about 150 mm in diameter and 140 mm in height. At the bottom of the target, we use a beryllium foil (125 mmϕ $\times$ 400μm thick) to reduce multiple scattering. The main contribution to the kaon multiple scattering comes from this window, at the level of which kaons have the lowest momentum. The side wall has eight windows open to the CCD units. Each CCD detector system has two CCD units of 17 $\times$ 26 mm^2 effective area. The window is a little larger (19 $\times$ 28 mm^2) than the effective area of a CCD, to keep tolerance for misalignments and to gain in solid angle. The material of the window is tentatively assigned to be Kapton; it is necessary however to make a detailed study of various materials (Kapton, Uplex, Be, etc.) to find the strongest material with the smallest deformation. The deformation of the window defines the distance between the target and CCD detectors, which is essential to the CCD solid angle. The center of the CCD system is 209 mm from the beam-beam interaction point.

The target is surrounded by a radiation shield to reduce helium consumption. For reducing heat conductance and for precise positioning, we use G10 to support the target. The radiation shield is vertically supported from the top flange of the cryostat with adjustable screws while horizontally it is supported by the side ring attached to the square shaped bottom flange of the upper vacuum vessel. The target is suspended by the radiation shield. Its suspension mechanism is a little bit complicated in order to reduce the heat conductance and to keep the maintenance capability. We cool down the target and the radiation shield by using liquid helium. The helium is transferred with an aluminum pipe, which is glued on the side wall of the target and its return gas flows through another pipe on the radiation shield. These pipes are connected by SUS flexible tubes, which also reduce heat conductance. The temperature of the target is controlled by the helium flow, either by flow controlling in the transfer tube or with active pressure control of the helium dewar. With this set-up, together with suitable insulators, we estimate the helium consumption to be few liters per day.

Chapter 5

Kaonic X-ray intensities

The intensity distribution of the K^-p X-rays is calculated by assuming that the atomic capture occurs at n=25 and with angular momentum l distributed statistically. Then the radiative transition rates are calculated to give the probability of observing a particular transition in the cascade.

For neutral exotic atoms such as $\pi^-\ p$, K^-p, $\bar{p}p$, collisional Stark mixing introduces an important density dependence to the X-ray yields. The strong electric fields seen in atomic collisions induce $nl \rightarrow\ nl \pm 1$ transitions. These are calculated using the model of Borie and Leon [1]. In the model, the strength of the Stark effect is adjusted by two parameters: the Stark mixing coefficient (k_{STK}) and the kinetic energy of kaonic hydrogen atom when it is formed (T). The parameters k_{STK} = 1.88 and T=1 eV give a good description of the π^-p and $\bar{p}p$ intensities.

Also required for this calculation are the strong interaction shifts and widths of the levels. Only the $1s$ and $2p$ values are significant; we estimate these from kaonic atom systematics [2]. The strength of the absorption from the ns levels are calculated by scaling the $1s$ absorption according to the ratio of the density of the Coulomb wave functions at the nucleus. A similar scaling from the $2p$ level absorption is used for the absorption from the np levels. As a consequence, if the $2p$ width is large, the intensity of the K_α and K_β lines will be reduced. In Table 5.1 are given the expected X-ray yields for the configuration, together with some variations of these parameters in order to estimate the sensitivity of the result. Fig 5.1 shows the expected K^-p X-ray complex with the resolution of the CCD detectors included. It should be noted that the entire complex is fit to determine the X-ray shift and width. Thus, in the event that the K_α strength is reduced, the remainder of the complex will fix the strong interaction parameters, albeit with somewhat larger systematic errors. The ratio of L to K X-rays will determine Γ_{2p}.

For kaonic deuterium there is a very considerable variation of the strong interaction parameters depending whether they are taken from phase shifts or kaonic atom

Table 5.1: Calculated X-ray intensities for Kaonic hydrogen and deuterium

P (atm)	k_{STK}	T (eV)	Δ_{1s} (eV)	Γ_{1s} (eV)	Γ_{2p} (meV)	K_α (%)	K_β (%)	$K_{>\beta}$ (%)	L_α (%)	L_β (%)	L_γ (%)	L_∞ (%)
Kaonic hydrogen												
36	1.88	1	-100	400	.1	4.5	2.6	8.2	2.3	2.8	1.9	0.8
36	1.88	1	-100	400	.5	1.4	1.0	5.8	1.0	1.7	1.6	0.7
10	1.88	1	-100	400	.1	7.3	3.3	12.5	3.6	3.0	3.5	2.3
36	1.88	1	-100	200	.1	4.1	2.2	7.3	2.0	2.5	1.7	0.7
36	1.88	.3	-100	400	.1	6.4	3.7	11.3	3.3	4.0	2.7	1.0
Kaonic deuterium												
36	1.88	1	-450	650	1.7	0.3	0.2	2.7	0.3	0.4	0.8	0.7
36	1.88	1	-550	980	24.5	0.0	0.0	0.3	0.0	0.0	0.1	.25

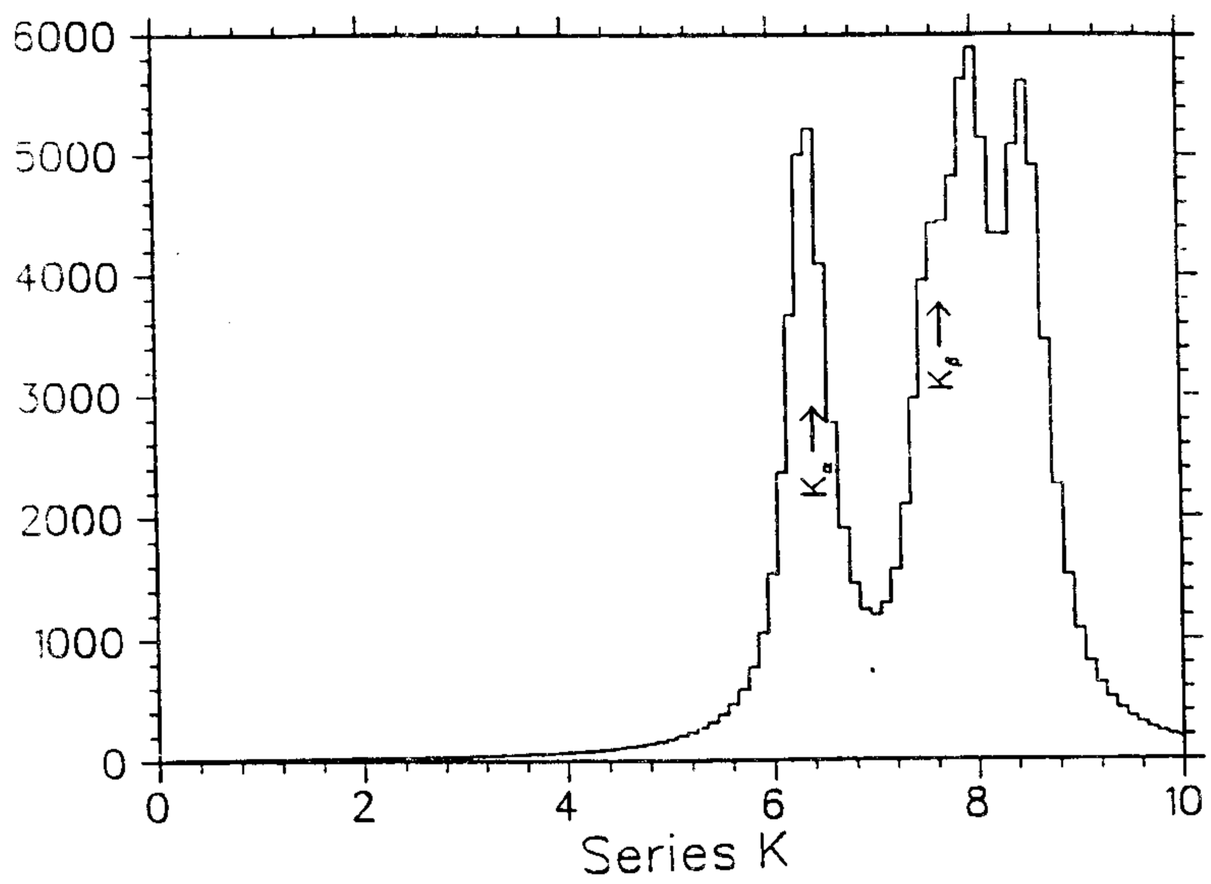

Figure 5.1: The K^-p X-ray complex peaks, with the CCD resolution included

systematics. This measurement is much more difficult than in hydrogen, and is not possible for the KEK experiment (see Chapter 7).

Bibliography

[1] E. Borie and M. Leon, Phys. Rev. **A21** (1980) 1460.

[2] C.J. Batty, Nucl. Phys. **A372** (1981) 418.

Chapter 6

The simulation program

6.1 Introduction

The simulation of the proposed experimental set-up for the DEAR experiment was performed with a Monte Carlo program in the framework provided by the CERN simulation package GEANT3 [1], using the version 3.21 of the code.

The Monte Carlo program was mainly finalized to simulate the physical processes involved, in order to optimize the experimental set-up as far as geometry (dimensions, materials, etc.) and performance (counting rate, background contamination) are concerned. All the relevant physical volumes of the apparatus, the detector structure, as well as the mechanical walls and supports interposed in the particle paths were modelled with appropriate level of detail. Also the relevant elements of the DAΦNE interacting region (pipe geometry and structure, Be window dimensions and thickness) were included in the Monte Carlo.

The program generates the primary ϕ-mesons produced by the e^+e^- collisions, taking into account the electron and positron energy spread and the beam dimensions in the crossing point, according to the parameters expected for DAΦNE. The generated ϕ's are then allowed to decay in all their relevant final states, according to the corresponding branching ratios:

$$\begin{aligned} \phi \rightarrow \quad & K_s^0 + K_L^0 \quad (34.4\%) \\ \rightarrow \quad & K^+ + K^- \quad (49.1\%) \\ \rightarrow \quad & \rho + \pi \quad (12.9\%) \\ \rightarrow \quad & \pi^+ + \pi^- + \pi^0 \quad (2.40\%) \end{aligned}$$

The decay particles are then transported through the materials of the experimental set-up, allowing them, apart from the processes of energy loss and multiple scattering, to decay or interact both electromagnetically (e.m.), eventually generating e.m. showers, and hadronically. When a K^- is stopped in the target, its hadronic

interaction at rest with the proton is switched on using *dedicated routines*, according to the following reactions:

$$\begin{aligned} K^- + p \rightarrow \quad & \Lambda + \pi^0 \quad (7.5\%) \\ \rightarrow \quad & \Sigma^+ + \pi^- \quad (19.6\%) \\ \rightarrow \quad & \Sigma^- + \pi^+ \quad (46.7\%) \\ \rightarrow \quad & \Sigma^0 + \pi^0 \quad (26.1\%) \end{aligned}$$

and for other materials the corresponding reactions on a neutron.

Moreover, an X-ray photon of 6.5 KeV is also generated when the stopping point is inside the target, to simulate the emission of X-rays from the formation of kaonic-hydrogen.

Finally, all particles which hit the CCD detectors are recorded, in order to extract all the relevant information: type of particle, deposited energy, momentum spectrum, and so on.

6.2 The DEAR Monte Carlo program

The performance of the experimental set-up, both regarding the counting rate of "signal" photons (6.5 KeV), emitted after the formation of kaonic-hydrogen, and the signal to background ratio, where background photons are soft (less than 10 KeV) X-rays, depends critically on the *reliability of the code at very low energies.* In particular, *the behaviour of photons, electrons and positrons must be accurate below the minimum low energy cut-off (10 KeV) of the standard GEANT package.*

For energies below few tens of KeV the photoelectric process is the most relevant one. We have verified that the interaction cross sections used in the GEANT program remain accurate at very low photon energies, i.e. also photons below 10 KeV are correctly propagated through materials.

In fig. 6.1 and fig. 6.2 the photon mass attenuation length [2] and photon interaction cross section [3] as a function of the photon energy, starting at photon energy of 1 KeV, are plotted for hydrogen and different materials, and silicon, respectively.

In the figures, the literature values of the cross section and the values used inside the GEANT code are compared. As seen, there is a nice agreement between literature values and those used in the Monte Carlo: in particular, the absorption peak in Si at 1.87 KeV is very well reproduced.

Electrons and positrons can generate photons by the bremssthralung process. This process has the well known "infrared" catastrophe, and hence could potentially produce hazardous (less than 10 KeV) X-rays. In the GEANT package, the

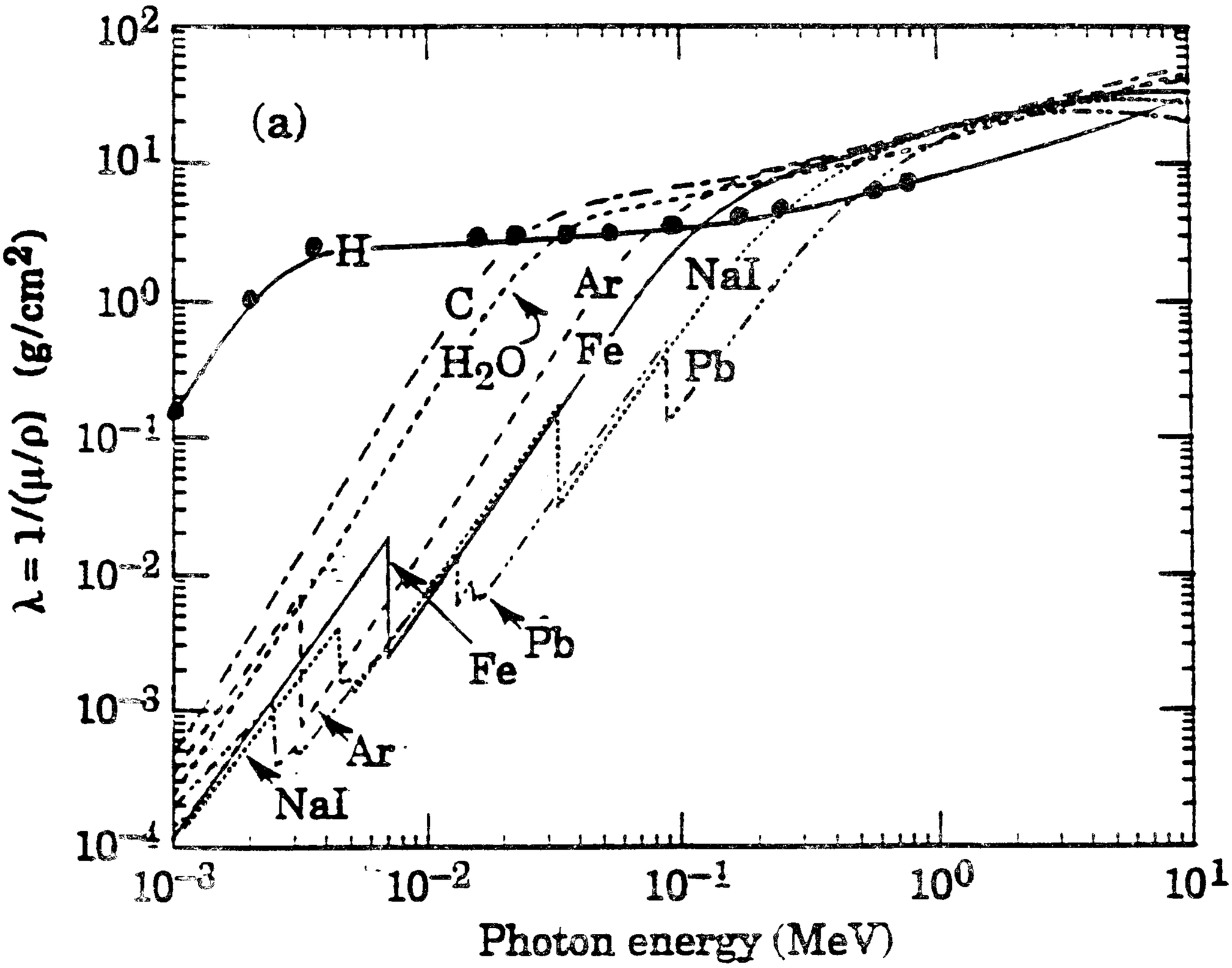

Figure 6.1: The photon mass attenuation length as a function of the photon energy, for hydrogen and different materials [2]. The black dots correspond to the values used in GEANT for hydrogen.

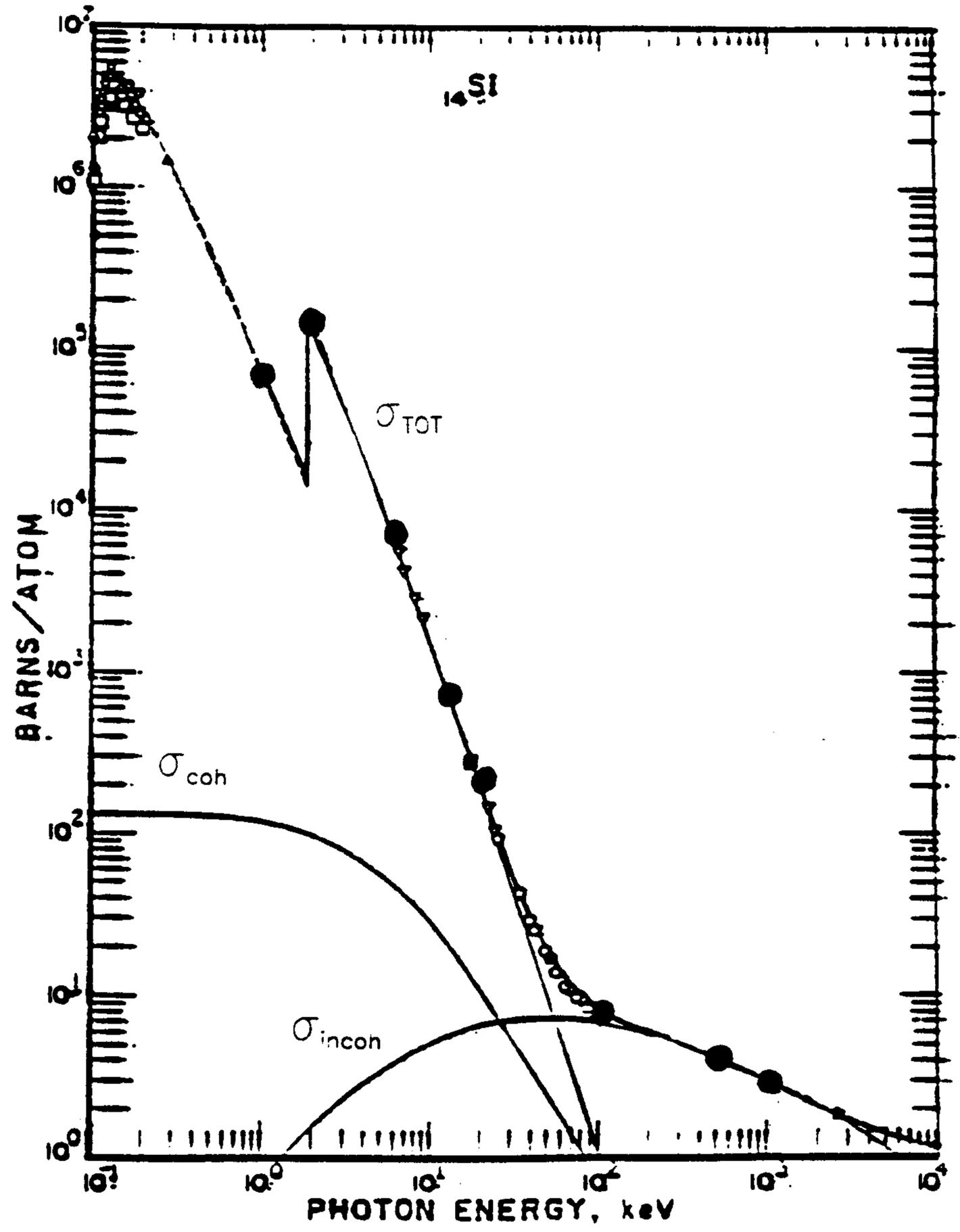

Figure 6.2: The total photon interaction cross section as a function of the photon energy for Si [3]. The black dots correspond to the values used in GEANT for silicon.

bremsstrahlung process is treated in three different routines: GBRELE,GBREME and GBRSGE, which all are based on the bremsstrahlung cross section values tabulated in the paper of S.M. Seltzer and M.J. Berger [4], for all materials and for electron energies from 1 KeV up to 10 GeV. In all the mentioned routines a fundamental role is played by the parameter k_c, which is the low energy cut-off. It is the photon energy below which the bremsstrahlung process is treated only as a continuous energy loss of the electron (positron), to be summed up to the ionization energy loss (routine GBRELE). Above k_c, the bremsstrahlung photon is generated according to the energy/angular distribution of the bremsstrahlung process by the routine GBREME. To calculate the total cross section of bremsstrahlung, for an electron (positron) of kinetic energy T, travelling in a given material, for emission of a photon with any energy above k_c and below T, the routine GBRSGE is used in GEANT.

We have verified, for different materials, electron kinetic and photon cut-off k_c energies, that the values calculated in the GEANT routines GBRELE and GBREME are accurate down to 1 KeV by comparing their calculated values with the corresponding ones reported in the tabulation given in the paper of S.M. Seltzer and M.J. Berger [4]. As an example, in fig. 6.3 the bremsstrahlung photon spectrum calculated by the routine GBREME for electrons of kinetic energy 5 KeV propagating in Al is compared with the values given in the S.M. Seltzer and M.J. Berger tabulation [4]. The agreement is very good.

On the other hand, the total cross section values calculated by the GEANT routine GBRSGE are unreliable when the cut-off parameter k_c is put below 10 KeV. This can been seen in fig. 6.4, where the total bremsstrahlung cross section in hydrogen, integrated over the photon energy from k_c up to the maximum, is shown as a function of the electron kinetic energy T, for different values of k_c, as calculated by the routine GBRSGE. As one can see, the points corresponding to $k_c = 2$ KeV show an unphysical peak for T around 100 MeV.

To recover the expected logarithmic increase of the cross section as a function of the electron energy T also when k_c is less than 10 KeV, *we modified the GBRSGE routine, for k_c below 10 KeV, in such a way that the total bremsstrahlung cross section values σ follow the law*:

$$\sigma = \alpha(k_c) + \beta(k_c)\log(T)$$

The values of the parameters $\alpha(k_c)$ and $\beta(k_c)$ were obtained from a fit of the cross section values above k_c=10 KeV. We estimate that this approximation is not worse than the 10-15% error quoted for the GEANT code between 10 KeV and 1 MeV.

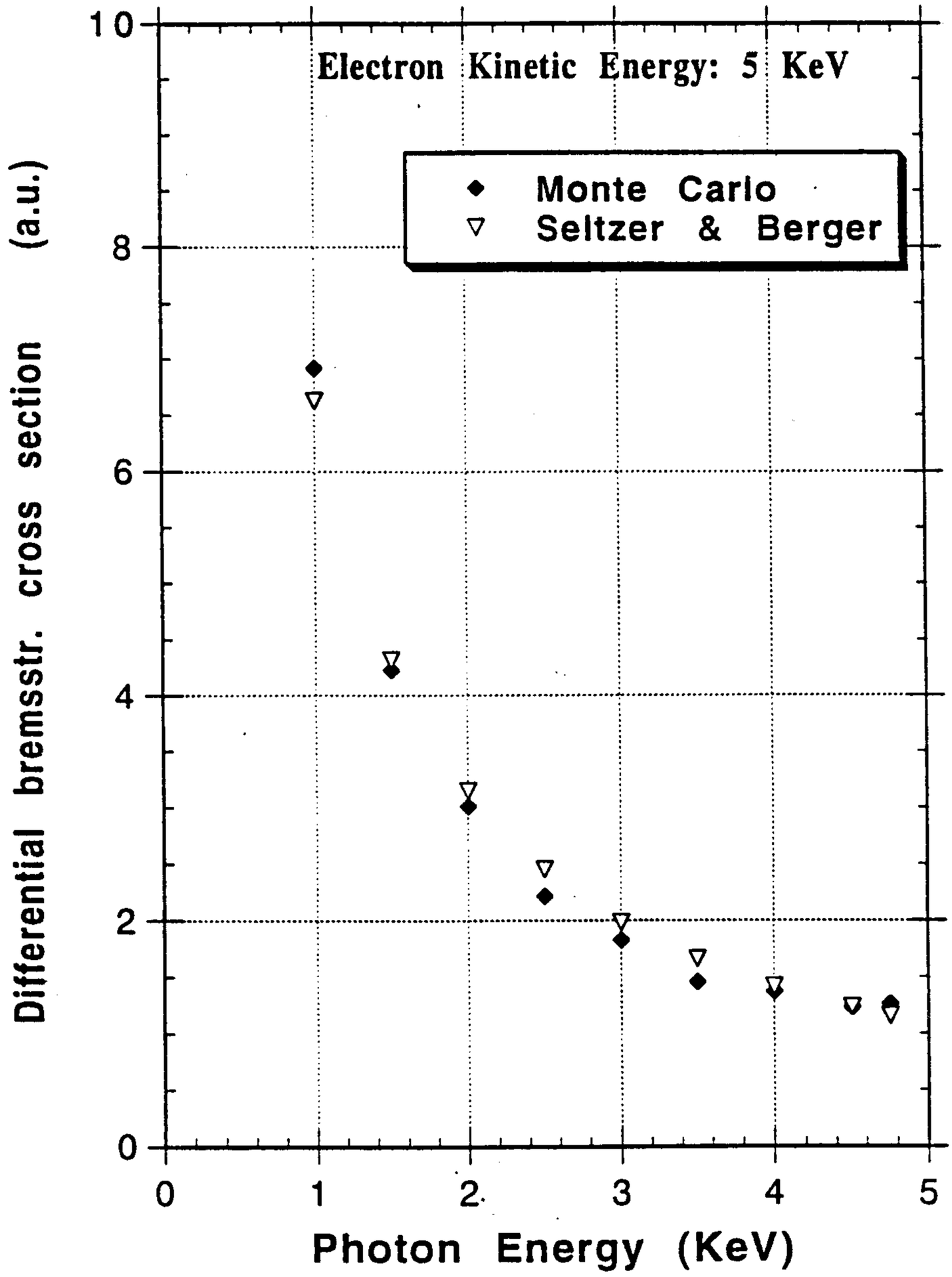

Figure 6.3: The bremsstrahlung cross section, differential in the photon energy, for 5 KeV electrons in Al, as tabulated in the paper of Seltzer and Berger [4] (open diamonds), in comparison with the GEANT calculation (closed rombs).

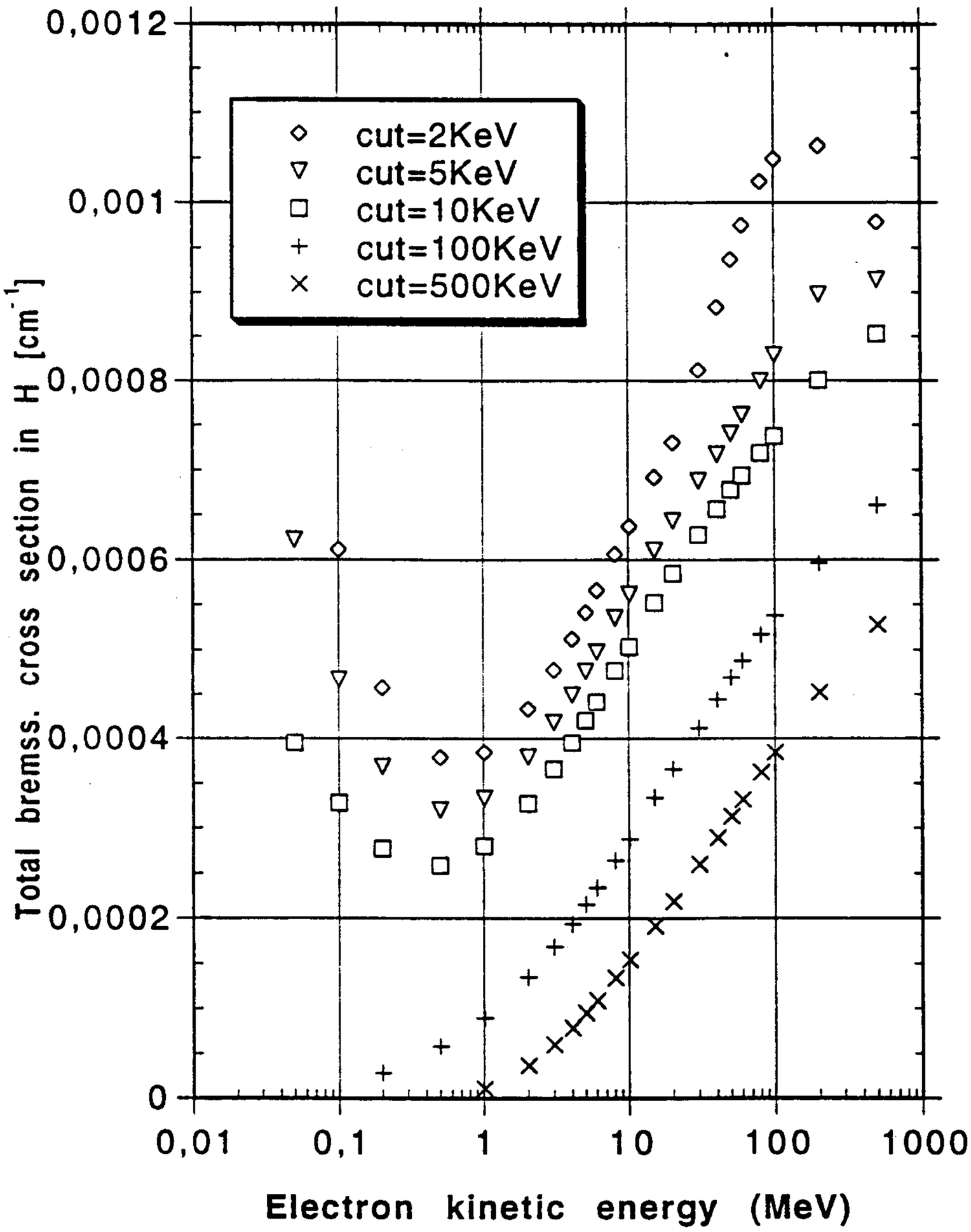

Figure 6.4: The total bremsstrahlung cross section in hydrogen, as a function of the electron kinetic energy, for different values of the cut-off energy, as calculated by the routine GBRSGE. The points corresponding to the cut k_c=2 KeV show an unphysical peak for electron kinetic energy around 100 MeV.

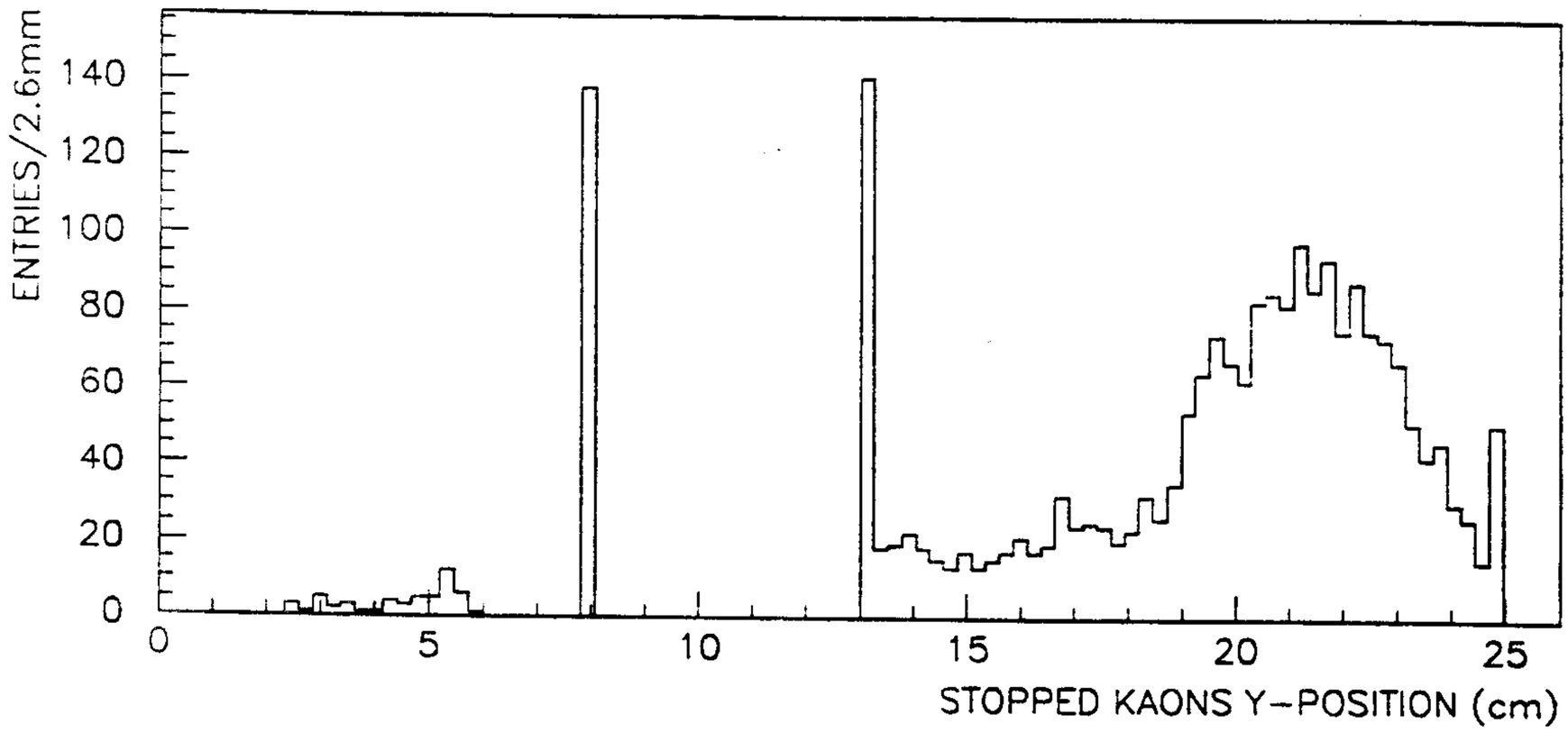

Figure 6.5: y coordinates of the stopped kaons. The different peaks correspond to kaons stopped in the various materials: 2.1 mm plastic degrader (at y=5.4 cm), 0.4 mm Al window of the vacuum box (y= 8 cm), 0.4 mm Be entrance window of the target cell (y=13 cm) and 3 mm Al top window of the target cell (y=24.5 cm). The broad distribution between y=13 cm and y=24.5 cm corresponds to kaons stopped in the hydrogen inside the target cell.

6.3 Physics performance

Using the Monte Carlo code, the physical performance of the proposed DEAR apparatus has been calculated, and is summarized in the following paragraphs.

6.3.1 Kaon stopping points

The profile, along the positive y-axis, of the distribution of the K^- stopping points inside the apparatus is shown in fig. 6.5. It is possible to see the various peaks, corresponding to kaons stopped in the different windows, and the broad peak corresponding to kaons stopped in the hydrogen target. In fig. 6.6 a bidimensional plot of the kaon stopping points is also shown.

The selected geometry allows stopping inside the cryogenic hydrogen target of a 3.4% fraction of all the charged kaons produced from ϕ's decay.

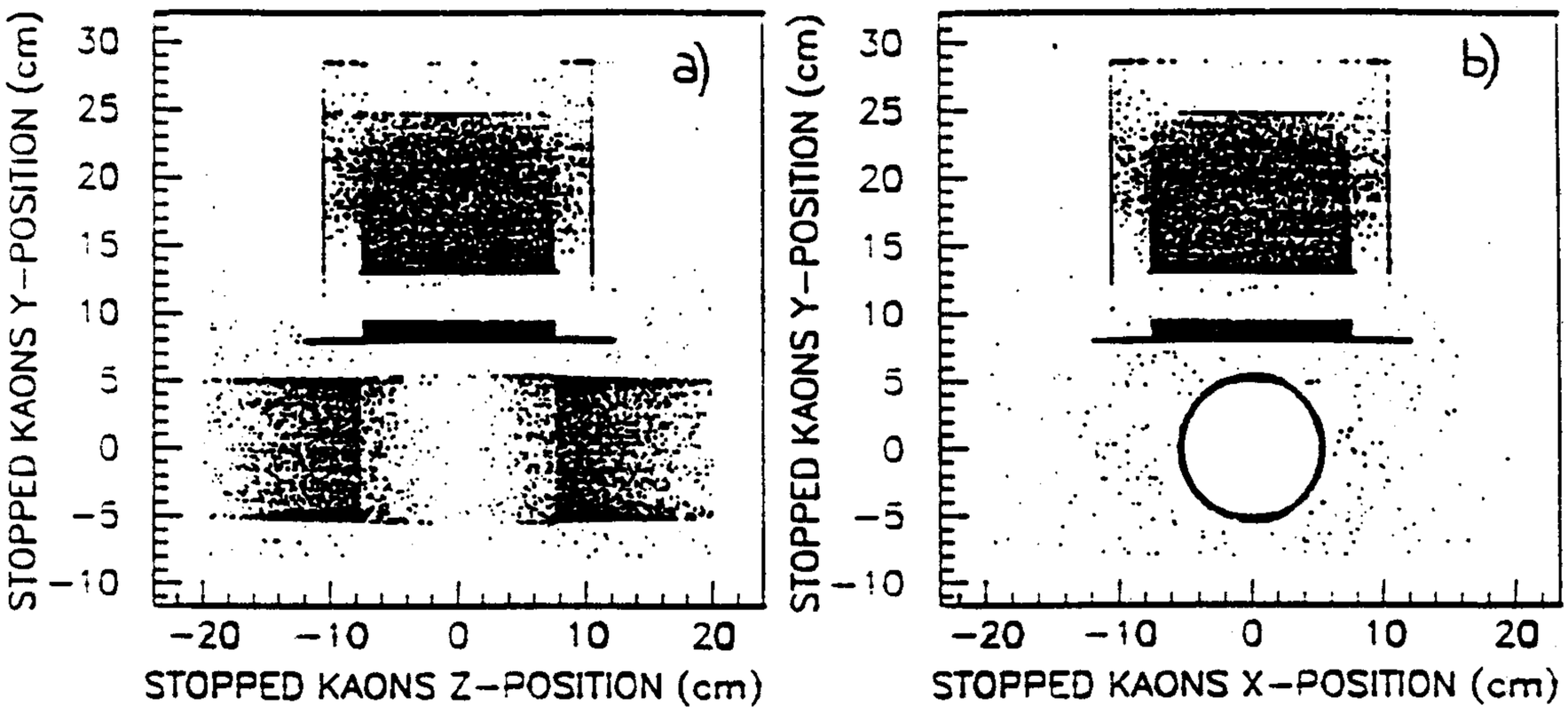

Figure 6.6: Bidimensional distribution of the kaon stopping points. In a) is shown the y versus z distribution for any x, and in b) the y versus x distribution for any z. The pipe, the Al vacuum box, the target cell and the windows are clearly seen, together with the target volume. It should be remembered that K^-s from ϕ decays are not a directional beam, but are emitted in the whole solid angle.

6.3.2 Momentum spectra

The momentum distribution of the different particles hitting the CCD detectors is shown in fig. 6.7 (π^+), 6.8 (π^-), 6.9 (μ^+), and 6.10 (photons).

As it is seen, the peaks in the π^+ spectrum at 182 MeV/c, due to the reaction $K^-p \rightarrow \Sigma^-\pi^+$ and the one at 205 MeV/c, due to the decay $K^+ \rightarrow \pi^+\pi^0$; the peak in the π^- spectrum at 173 MeV/c due to the reaction $K^-p \rightarrow \Sigma^+\pi^-$; the peak in the μ^+ spectrum at 230 MeV/c due to the decay $K^+ \rightarrow \mu^+\nu_\mu$; and the 511 KeV/c photon peak due to positron annihilation at rest, are all clearly reproduced.

6.3.3 Counting rate

In the experimental set-up described in Chapter 2, the number of 6.5 KeV obtained X–rays, deriving from kaonic-hydrogen formation, which hit the 8 CCD detectors is 765 for 1100000 generated ϕ's. The measured CCD efficiency for 6 KeV photons is about 60% (well reproduced by our Monte Carlo, which gives, for the $30\mu m$ depletion layer of the CCD used in the simulation, a "physical" efficiency of 65%). Supposing a yield of 3% for 6.5 KeV K_α X–rays from kaonic-hydrogen (from the cascade calculation reported in Chapter 5 with the selected conditions of pressure and temperature (hence density) of the hydrogen target) and a DAΦNE luminosity of $10^{32}s^{-1}cm^{-2}$, the expected counting rate is about *20 X-rays per hour*. Due to the CCD resolution at this X-ray energy (about 150 eV), these 20 X-rays in one hour

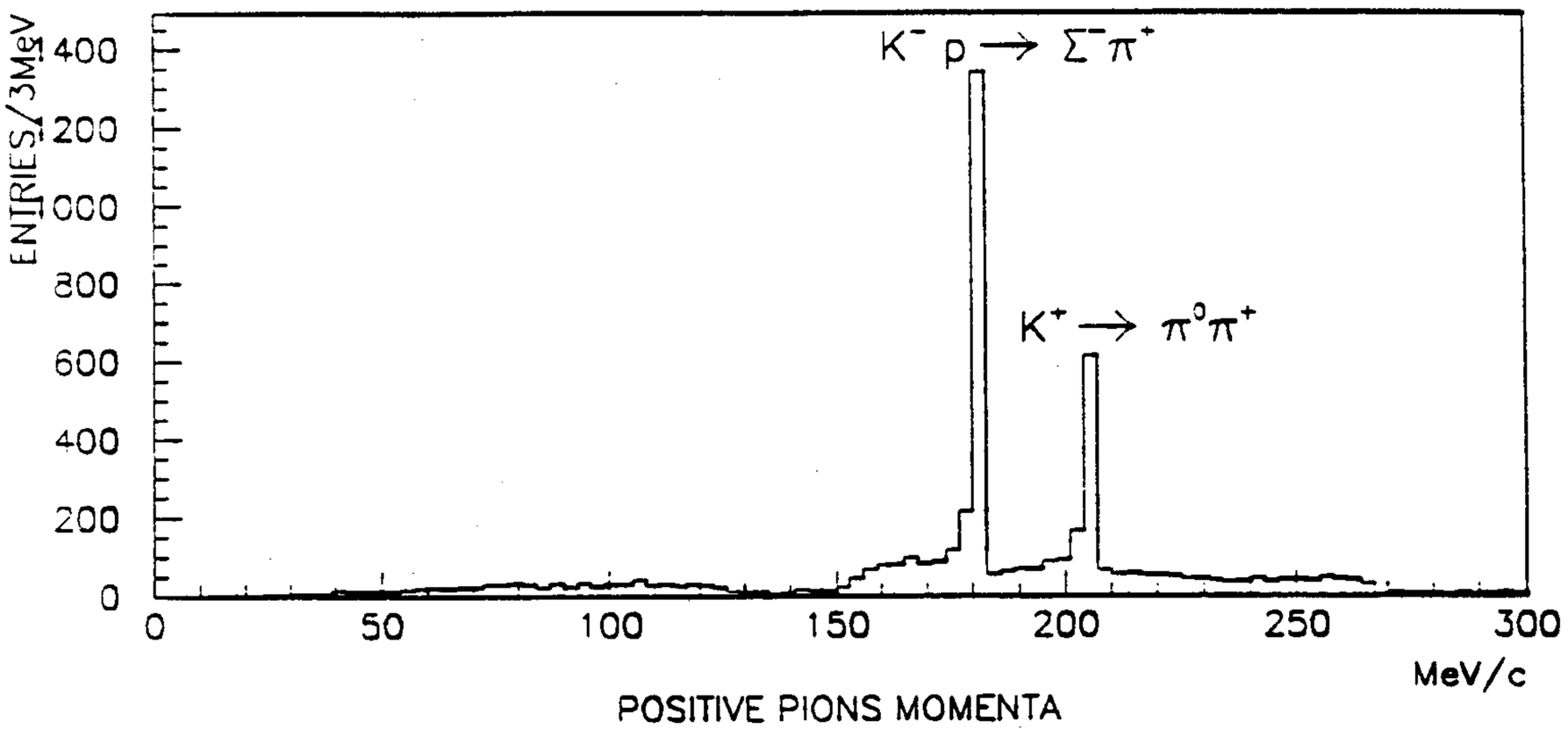

Figure 6.7: Momentum distribution of positive pions that hit the CCDs. The peak from the reaction $K^- p \rightarrow \Sigma^- \pi^+$ at 182 MeV/c and the peak from the decay $K^+ \rightarrow \pi^0 \pi^+$ at 205 MeV/c are clearly seen.

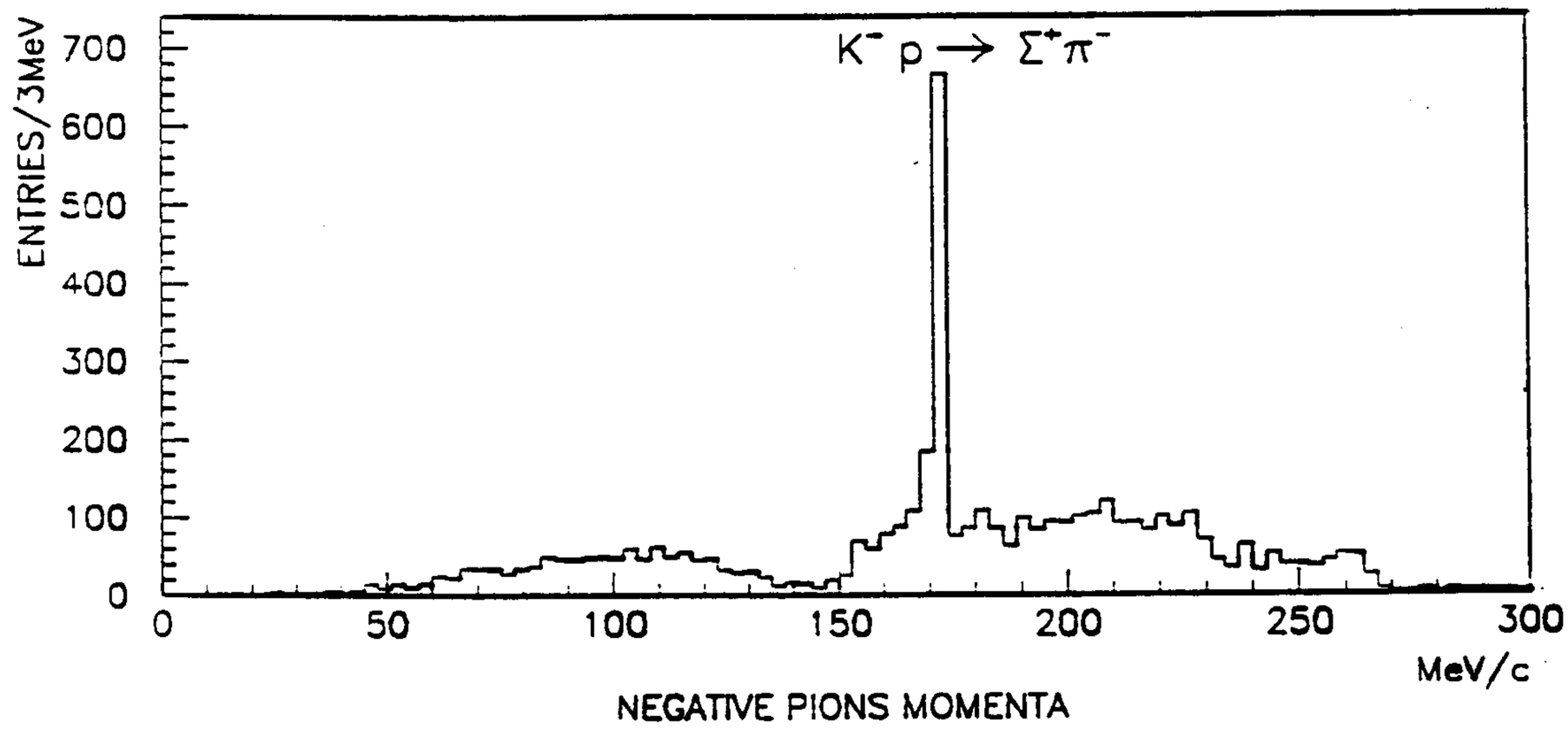

Figure 6.8: Momentum distribution of negative pions that hit the CCDs. The peak at 173 MeV/c is due to the reaction $K^- p \rightarrow \Sigma^+ \pi^-$.

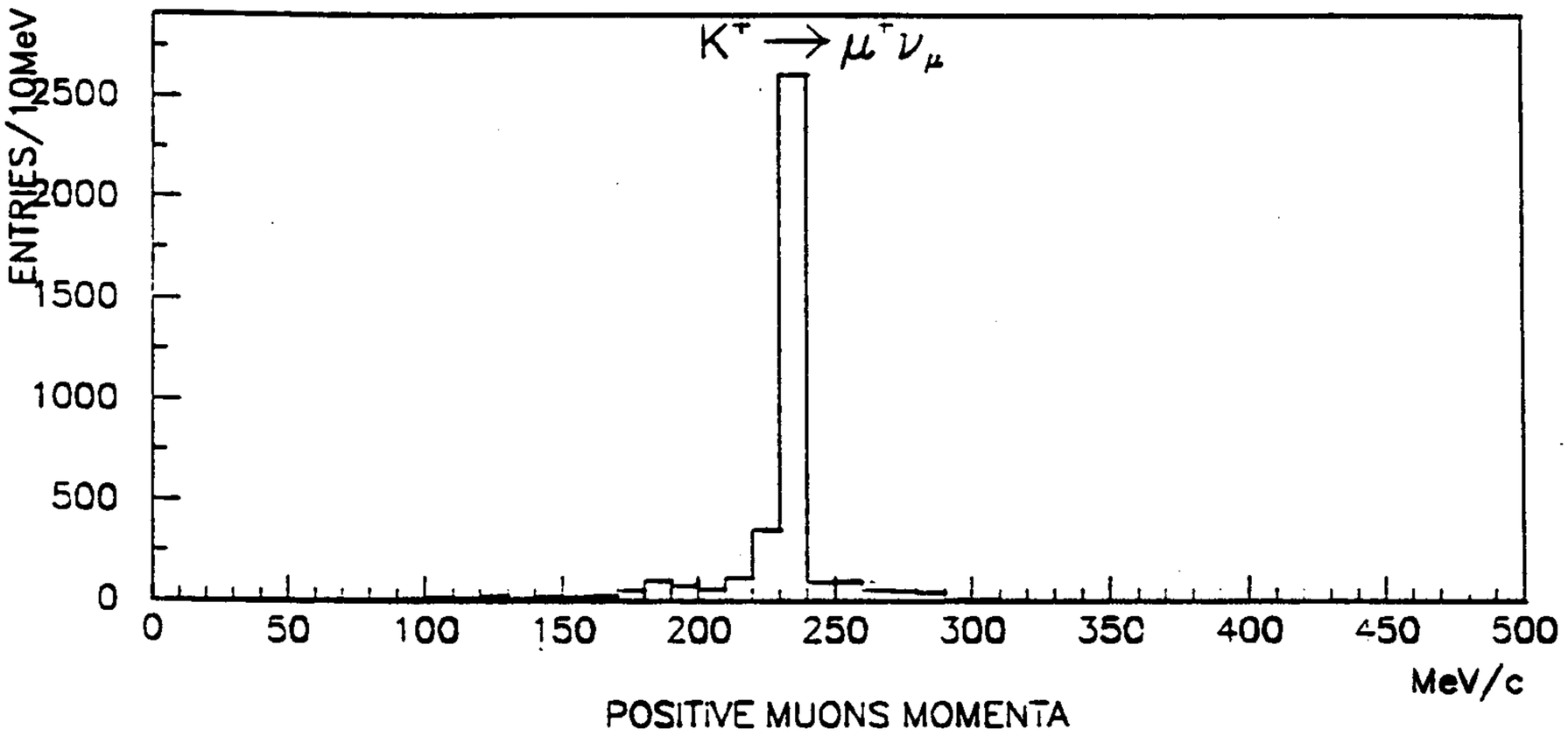

Figure 6.9: Momentum distribution of positive muons hitting the CCDs. The peak at 230 MeV/c is due to the decay of $K^+ \rightarrow \mu^+ \nu_\mu$.

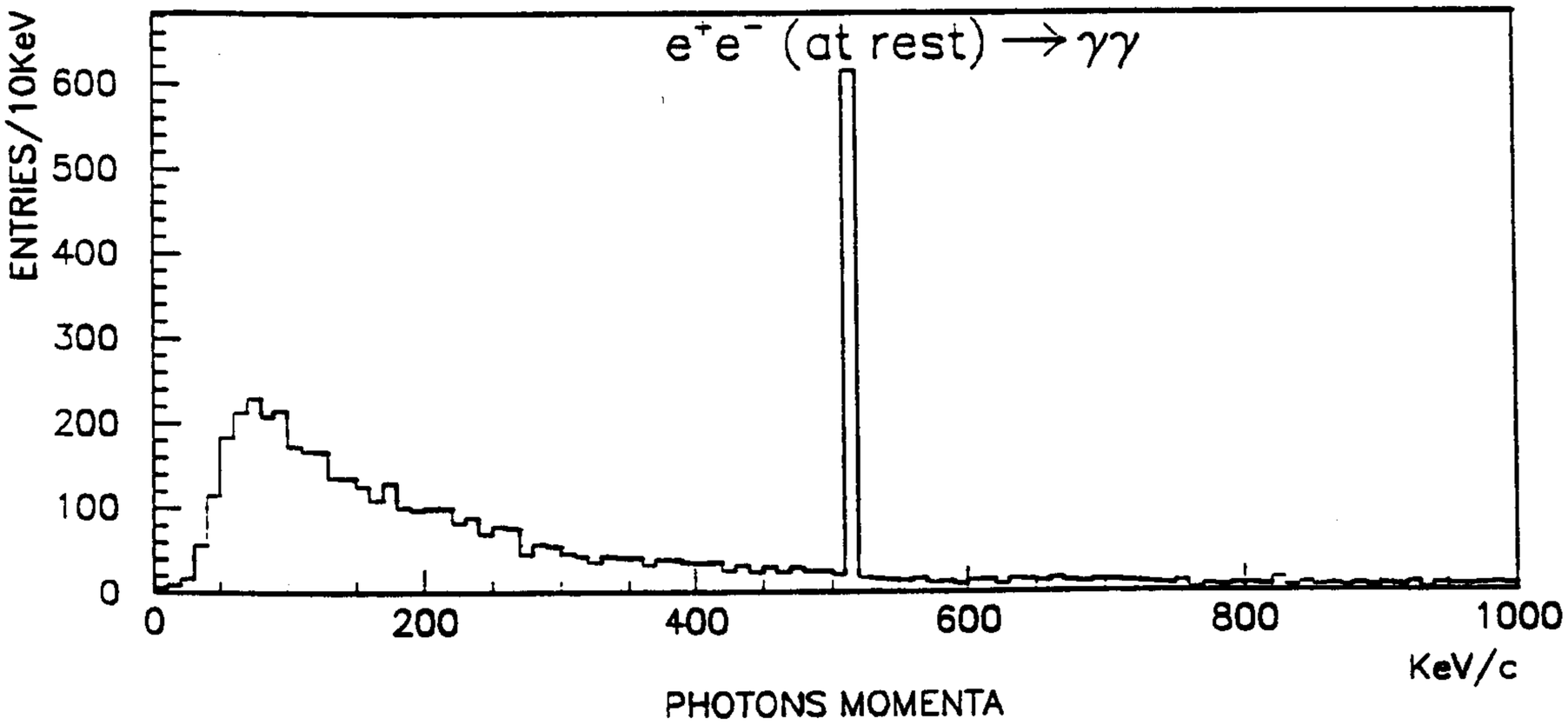

Figure 6.10: Low energy part of the momentum distribution of photons hitting the CCDs. The peak at 511 KeV/c is due to the two photons resulting from positron annihilation at rest.

are expected to be spread out, within $\pm 2\sigma$, in 4 channels of 100 eV width around 6.5 KeV, if we assume an intrinsic width $\Gamma_{1s} = 200$ eV ($\Gamma_{tot} = 250$ eV $\sigma \simeq 100\,eV$). If $\Gamma_{1s} = 400$ eV ($\Gamma_{tot} = 420$ eV $\sigma \simeq 180$ eV), the signal is spread over 4 channels, within $\pm$ 1.2 σ, or over 7 channels, within $\pm$ 2 σ.

6.3.4 Background evaluation

The background on CCDs can be divided in two categories: the first affects the operational conditions of a CCD causing its "blindness", i.e., it is connected to the maximum number of pixels which can be involved in a CCD avoiding "double hits" (in the sense explained in Chapter 3). This background is directly given by the number of ionizing particles which hit the surface of a CCD (or, better, half a CCD, since the readout takes into account half a CCD). The second category of background is represented by the hits of soft X-rays (below 10 KeV) which affect signal identification and peak resolution.

The background particles can have, in turn, two origins: particles generated by the hadronic interaction of the stopped K^- ("hadronic background"), and "machine background" generated by the electrons and positrons lost from the primary beams circulating in $DA\Phi NE$. This last type of background has two main sources: primary particles lost by the Touschek effect and primary particles lost by beam-gas interaction (Coulomb scattering and bremsstrahlung on the residual gas inside the pipe).

Hadronic background

As noted, each stopped K^- has a hadronic interaction at rest with the protons of the target and with the protons and neutrons of the target materials (walls, windows, etc.). As a result of these interactions, "hadronic" particles are produced which can hit the CCDs, depositing energy in them, or, as for the case of photons coming from π^0s decay, initiating an e.m. shower which can produce soft X-rays hitting the CCDs. With the Monte Carlo program, we generated 1100000 ϕ's, corresponding to 42 *min* of beam time at a luminosity of $10^{32} s^{-1} cm^{-2}$ and obtained 10190 ionizing hits on CCDs and 5 X-rays below 10 KeV.

The 10190 ionizing hits on CCDs in 42 *min* correspond to a blindness of 4.07 $part.s^{-1}$ on 8 CCDs (overall surface $\cong$ 36 cm^2), equivalent to 0.113 $part.cm^{-2}s^{-1}$, which means 0.25 $part.s^{-1}$ on 1/2 CCD.

The 5 X-rays below 10 KeV on CCDs in 42 *min* correspond to 0.07 background photons per channel of 100 eV per hour, which means 0.28 X–rays/h over 4 channels. This is equivalent to a background level of $\simeq$ 1.4% and to a signal/background ratio of about 71:1. This *low hadronic soft X-ray background on the CCDs* can be

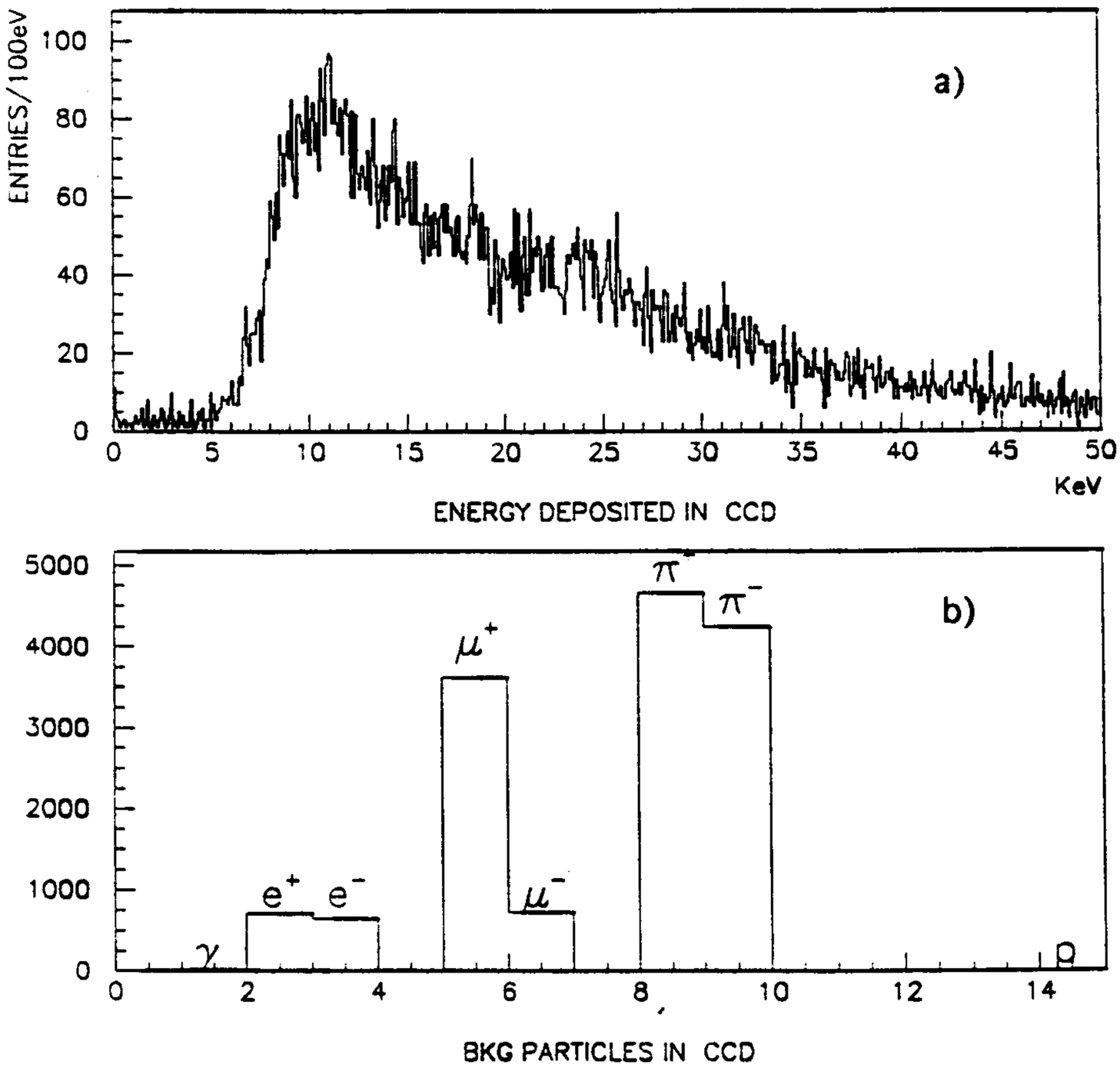

Figure 6.11: a) Energy deposition below 50 KeV in the CCDs; b) type of particles whose energy deposition in CCDs is less than 50 KeV.

explained by their very thin depletion layer ($30\mu m$), which prevents electrons or positrons to radiate inside the CCD. On the contrary, the usual Si detectors used in previous experiments on kaonic hydrogen (see Chapter 1) and in the present one at KEK (see Chapter 7), were affected by a very high hadronic background of soft X-rays. This was due to the large thickness (few mm), used in order to obtain 100% detection efficiency, which caused the detector itself to act as radiator for electrons and positrons. The different behaviour of CCD and Si 4 mm thick, as calculated by our Monte Carlo in the same conditions, can be seen in fig. 6.11 and fig. 6.12, respectively, which show the energy deposition and the type of responsible particle. As can be seen, the contribution of soft X-rays, negligible in CCDs, is most important in 4 mm Si.

Machine background

a) Background from Touschek effect

The Touschek background for the DEAR experiment was studied with the dedicated Monte Carlo program in the following configurations:

a.1. DAY-ONE configuration for a KLOE-type section, with the following parameters [5]:

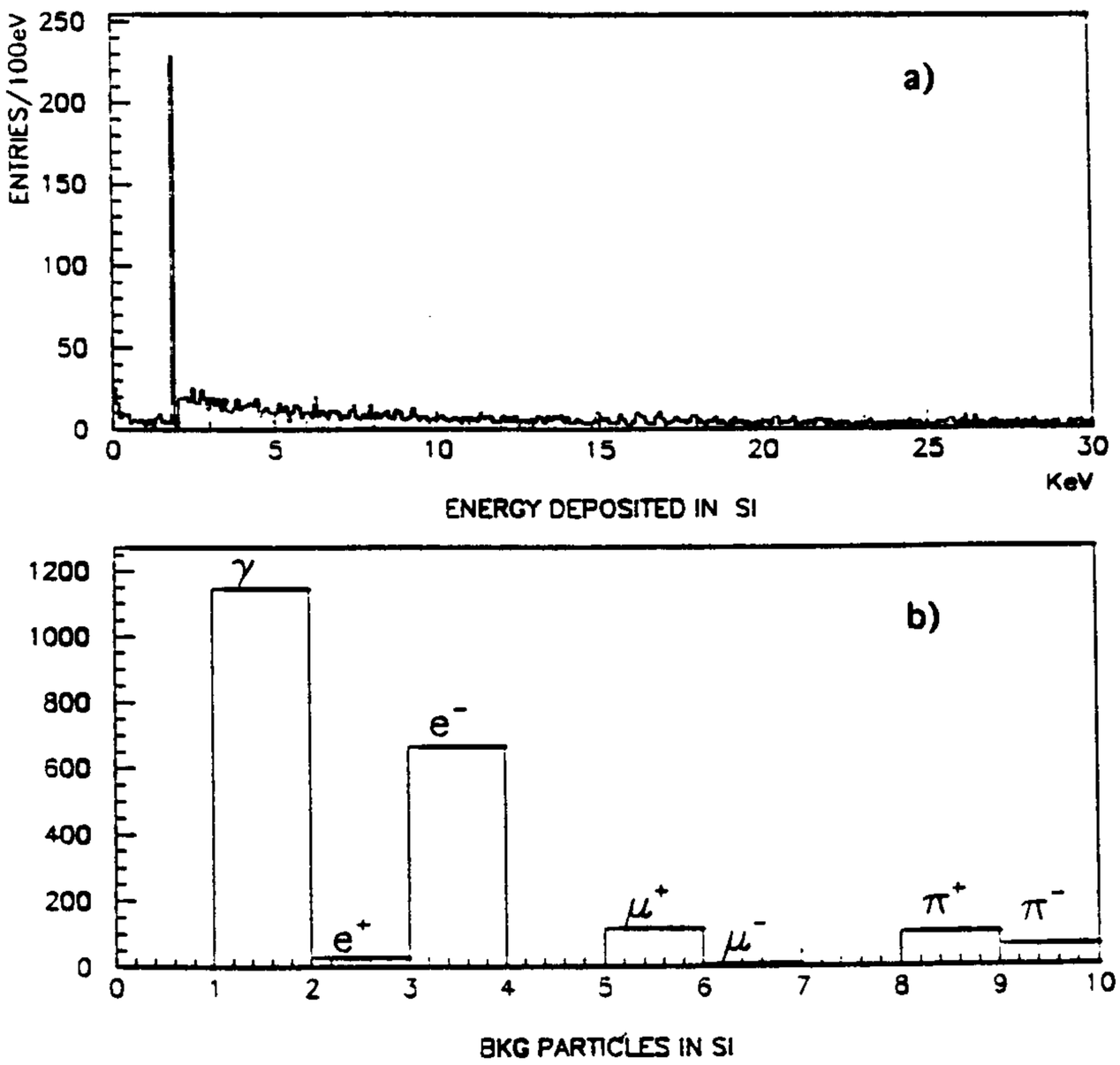

Figure 6.12: a) Energy deposition below 30 KeV in 4 mm Si; b) type of particles whose energy deposition in Si is less than 30 KeV.

- no central quadrupole;
- aperture of the first quadrupole of 43 mm
- scraper aperture of 9 σ_x
- 915 lost particles per second per beam per bunch
- $8.9 \cdot 10^{10}$ particles per bunch.

In this configuration the lost particles (electrons and positrons) are hitting the pipe with an angle of about 12.5 mrad, in the radial plane, having a distribution along the z-axis (beam-line) spread between (-75, -45) cm and (45,75) cm with respect to the impact point [5].

Using the DEAR Monte Carlo program the background coming from the Touschek effect was studied in the following way: 1 million electrons hitting the pipe with an angle of 12.5 mrad in the radial plane, in the region: (-75, -45) cm, (upstream), and having an uniform distribution along the z-axis were simulated. Their interaction (showers) with all the materials present in the experimental set-up were considered, the showers and all the particles created being followed down to 1 KeV, and all the particles hitting the CCD's being recorded.

The rate of lost particles under the conditions of $10^{32} s^{-1} cm^{-2}$ luminosity, corresponding to 30 bunches, is about 55 kHz, which means that the 1 million generated events correspond to a real time of about 18 seconds.

The following numerical results for the operational regime of CCD's (blindness of CCD's) were obtained:

- a total number of 1950 particles depositing energy in the 8 CCD's were obtained, which means:

- Number of particles/s over 8 CCD's = 108 part/s in 8 CCD's

- Number of particles/cm^2/s = 3.0 part/cm^2/s

- Number of particles/s over 1/2 CCD = 6.6 part/s over 1/2 CCD

a.2. DAY-ONE configuration for a KLOE-type section, with the optics parameters as follows:

- no central quadrupole

- aperture of the first pair of quadrupoles (low-beta) of 53 mm

i) scraper aperture of 9 σ_x

In this configuration, the resultant number of lost particles/s/beam/bunch is zero, so that the Touschek contribution at the level of the CCD's operational limit (blindness), as well as for the X ray background is zero.

ii) scraper aperture of 10 σ_x

In this configuration, the number of positive energy lost particles (those for which the relative energy change due to Touschek effect is positive) is zero, whereas for the negative energy lost particles (those for which the relative energy change due to Touschek effect is negative) the loss is 140 lost particles/s/beam/bunch. These particles are lost at 2.2 m from the interaction point (downstream). Since the lost particles are hitting the pipe far away downstream, their contribution can be considered negligible.

In summary: *for a 53 mm aperture, no background contribution due to Touschek effect has to be considered.*

b) Background from beam-gas interaction

As a starting point for the evaluation of the Coulomb scattering and beam-gas bremsstrahlung background the KLOE note by E. Gero [6] was used. In the report a study of this kind of background was done, with specific reference to the KLOE configuration. In this study the following conditions were considered: average vacuum of $4 \cdot 10^{-10}$ torr and 120 bunches circulating.

From the Gero tables [6], the rates of lost particles hitting the pipe in the region (-46,-10)cm from the interaction point (our region of interest) are:

- Rate of lost particles (charged) coming from Coulomb scattering at large angles: 6 KHz
- Rate of lost particles (charged) coming from Coulomb scattering at small and very small angles: 0 KHz
- Rate of lost particles (charged + photons) coming from hard beam-gas bremsstrahlu 6.2 KHz
- Rate of lost particles (charged + photons) coming from soft beam-gas bremsstrahlun 0.7 KHz
- Rate of lost particles (charged + photons) coming from very soft beam-gas bremsstrahlung: 0.8 KHz.

The previous rates take into account reduction of the rates resulting from introducing a scraper before the splitter (Appendix C of [6]). The total rate of Coulomb and beam-gas bremsstrahlung background turns out 13.7 KHz.

In the DEAR Monte Carlo program we simulated these effects by generating 6.5 million electrons uniformly hitting the pipe between 10 and 46 cm upstream the interaction point, with an angle distributed between 0.667 and 6 mrad. The resultant secondary particles were followed in the DEAR set-up, down to an energy of 1 KeV and all the particles arriving at the CCDs were registered.

We were considering the following two regimes:
1. The luminosity considered for the DEAR experiment of $10^{32} s^{-1} cm^{-2}$ (30 bunches) and a vacuum of $4 \cdot 10^{-10}$ torr, a situation in which the total rate of loss of particles via Coulomb scattering and beam-gas bremsstrahlung is 13.7/4 KHz = 3.4 KHz. The 6.5 million lost particles generated correspond then to a time of about 1900 seconds. The results are the following:

• Operational limit of CCD's (blindness of CCD's)

The total number of particles depositing energy in the CCD's is 10240, which means:

- Number of particles/s on 8 CCD's = 4.96 part/s

- Number of particles/cm^2/s = 0.14 part/cm^2/s

- Number of particles/s over 1/2 CCD = 0.30 part/s over 1/2 CCD

• X-ray background

A total number of 28 X-rays, with energy below 10 KeV, depositing their energy in the CCD's, were registered in 1900 seconds. This means that we have 0.28 X-rays/channel in 1900 seconds (channel bin 100 eV), or 0.5 X-rays/channel in one hour. Since our signal coming from kaonic hydrogen in one hour is about 20 X-rays, spread over 4 channels, the Coulomb and beam-gas bremsstrahlung X-rays integrated background is about 2 X-rays in one hour in 4 channels. This is equivalent to a 9% X-ray background with respect to the overall number of X-rays in the energy region and to a signal/background ratio of 10:1.

2. If one considers that the vacuum may not be optimal ($4 \cdot 10^{-10}$ torr) at the end of the commissioning, it is realistic to consider a more pessimistic evaluation, taking, for instance, the values of lost particles for the full luminosity of 120 bunches, instead of the figures for 30 bunches.

Under these conditions, which can be assumed as a realistic evaluation, we have seen that the rate of Coulomb scattering and beam-gas bremsstrahlung lost particles is 13.7 KHz, and the 6.5 million lost particles generated correspond to a time of about 480 seconds. The results of the Monte Carlo simulation are:

• Operational limit of CCD's (blindness of CCD's)

The total number of particles depositing energy in the CCD's is 10240 in 475 seconds, which means:

- Number of particles/s over 8 CCD's = 20 part/s

- Number of particles/cm^2/s = 0.56 part/cm^2/s

- Number of particles/s over 1/2 CCD = 1.2 part/s over 1/2 CCD

• X–ray background

A total number of 28 X-rays with energy below 10 KeV, depositing their energy in the CCD's, were obtained in 480 seconds. This means that we have 0.28 X-rays per channel in 480 seconds (channel bin 100 eV), or about 2 X-rays per channel in one hour. Since our signal in one hour is about 20 X-rays, spread over 4 channels, the Coulomb and beam-gas bremsstrahlung X-ray integrated background for 4 channels is about 8 X-rays in one hour. This is equivalent to a 29% X-ray background with respect to the overall number of X-rays in the energy region and to a signal/background ratio of 2.5:1.

6.4 Conclusions

In conclusion, the DEAR Monte Carlo simulation program gives the following results, for a DAΦNE luminosity of $10^{32} cm^{-2} s^{-1}$:

- *K_α 6.5 KeV X-ray rate: about 20/hour*
- *Soft X-ray hadronic background: about 0.28/hour*
- *Soft X-ray machine background: about 8/hour*

  (worst case: bad vacuum conditions during the commissioning phase)
- *Hits depositing energy over half a CCD:*
  - *hadronic: about 15 part/min*
  - *machine: about 72 part/min*
  - *total: about 90 part/min, corresponding to a time of 50 min for reaching 4500 hits over half a CCD(max occupancy after which CCD readout is necessary: 4000-5000 hits over half a CCD, i.e. 20.000–25.000 pixels involved).*

Bibliography

[1] R. Brun, F. Bruyant, M. Maire, A.C. McPherson and P. Zanarini, GEANT3, CERN Report DD/EE/84-1 (1987) 1.

[2] L. Montanet *et al.*,Phys. Rev. D,*Review of Particles Properties* Vol.**50** (1994) 1259.

[3] J.H. Hubbell, Nat. Bur. Stand. (U.S.), Spec. Publ. **461** (1977) 3.

[4] M.Seltzer and M.J.Berger, Nucl. Instr. and Meth. **B12** (1985) 95.

[5] S.Guiducci, *Background evaluation in DAΦNE*, addendum to DAΦNE Technical Note **IR-6** (1995).

[6] E.Gero, *Beam-gas background calculation for DAΦNE*, KLOE Note **102**, (1994).

Chapter 7

Comparison with the KEK experiment

Very recently, a kaonic hydrogen X-ray experiment has been done at KEK (KpX : KEK-PS E228 experiment) [1].

To make a comparison with DEAR, let's start with a quick look at the KEK experimental condition. The KpX group uses a secondary kaon beam from the KEK 12 GeV proton synchrotron. A separated beam line is available, but the beam is largely contaminated by pions and only a few percent of the beam is kaons. The initial kaon momentum is 600 MeV/c to transport short-lived kaons through the long beam line. The detector used is composed of 60 large silicon counters Si(Li) (effective area 200 mm^2, thickness 5mm) for X-ray detection. Such a detector is not able to separate X-rays from very low energy charged particles and its resolution is about 400 eV (FWHM). There is also a large background due to the kaon interaction products. To overcome those severe conditions, the final state of the K^-p reaction, which is expected to be background-free, was selected (except for accidental background). This final state was selected by tagging two charged pions, so that the K^-p interaction point can be detected as a vertex point of the pion trajectories.

Thanks to DAΦNE, high purity and very low momentum monoenergetic kaons are available for the DEAR experiment. Because of these great advantages we can avoid many of the experimental difficulties which the KpX group must handle. Firstly, the DAΦNE kaon beam is not contaminated by a two–orders–of– magnitude–larger fraction of pions as is the case of KpX. Second, in DAΦNE, it is possible to stop kaons in the gaseous target system very efficiently, because of the monoenergetic very low momentum kaons. Actually, in DEAR a ten–times–larger percentage of kaons stop in the target per incident kaon, despite the more limited solid angle of the target with respect to the kaon source (electron-positron colliding point) than in the case of KpX. This fact compensates for the smaller kaon production rate (3000 kaons per second on average in KpX). Moreover, the spatial distribution of the stopped kaons in the DEAR target is quite small, so that the effective solid angle

per X-ray detector is very large.

These great advantages, and the much lower intrinsic background, open the way to use the world's best soft X-ray detector, the CCD, in the proposed experiment. As described in Chapter 3, the CCD has very high resolution and its background suppression procedure is well established. This detector can not be triggered, because of its long read out time, however the detector has already proved its ability in the $\bar{p}p$ X-ray experiment at LEAR, where the background contamination is more severe than in the present experiment. On the contrary, since the present experiment does not need a hardware trigger, we do not lose statistics by selecting the final state or through the efficiency of detecting the secondary particles, so that one order of magnitude larger statistics can be easily achieved. As a result, since the DAΦNE machine background is manageable, as it turns out from the Monte Carlo simulation (see Chapter 6), it is very probable that we will get an outstanding kaonic hydrogen K_α X-ray peak.

The KpX group is now in the analyzing phase, so that we can not discuss their results in detail at the moment. We can point out, however, what we can definitely improve in the DEAR experiment. First of all, due to the great improvement of the energy resolution, we can get more accurate results in shift and width. It should be pointed out also that we are able to measure kaonic deuterium X-rays with the same set-up.

KpX preliminary results show a kaonic hydrogen peak around 8 keV, which is assigned to be the superposition of transition lines to $1s$ state from $3p$ and higher states. This means that the energy shift is relatively small so that better resolution might be essential to determine its sign. The problem is that KpX finds only a weak enhancement around 6.5 keV, which corresponds to the K_α line ($2p$ - $1s$ transition). Thus it might be difficult to obtain shift and width of the $1s$ state from the 6.5 keV peak only. If this is the case, the KpX group must use the 8 keV peak to derive the physical quantities. This means that they might need to rely on atomic cascade calculations to know the relative intensities of each line. The result can be determined only within the uncertainties of the theoretical calculation.

In the DEAR experiment, with higher statistics and the better resolution of the X-ray detector, we can expect to observe the 6.5 keV peak more clearly and thus to obtain the strong shift and width of the $1s$ state with much less uncertainties.

Bibliography

[1] M. Iwasaki *et al.*, Nucl. Phys.**A585** (1995) 239c.

Chapter 8

Further perspectives

8.1 Light kaonic atoms

A straightforward extension of the kaonic–hydrogen experiment is to look for X–rays from kaons stopped in deuterium. Such a study would complement the data from hydrogen and could permit deduction of the scattering lengths below the $\overline{K}N$ threshold and, in combination with good K^-p data, might allow the K^-n scattering length to be determinated. The deuterium $2p$ - $1s$ X–ray energy is predicted to be 7.81 KeV, and again Stark mixing effects are expected to be large for a liquid target, although no detailed calculations are available. The energy shift and width predicted by Wyceh [1] are:

$$\varepsilon = -1.000\,eV \text{ and } \Gamma = 620\,eV$$

A typical feature of light kaonic atoms (He, Li, Be, etc.) is that the measured hadron shifts always turn out *negative*, i.e. the atomic bound states are repelled by the strong interaction. If the K^-p interaction is attractive, a systematic study of the strong interaction shifts in light kaonic atoms could indicate for which nucleus the strong interaction shift changes sign. The role of $\Lambda(1405)$ in the $\overline{K}N$ interaction could also be verified by looking for an eventual disappearence of the resonance for some light nuclei.

Bibliography

[1] S. Wycech, Preprint.

Chapter 9

Cost estimation, responsibilities, time schedule

9.1 Cost estimation

- *CCD detectors*

- n.8 CCDs ($4.5cm^2$) each \$ 11500 ..... \$ 92000

- command and readout electronics for 8 CCDs each \$ 4000 ..... \$ 32000

- VME and computer interface ..... \$ 15000

- PC, magneto-optic disk and printer ..... \$ 9000

- 10 rewritable optical disks 13 Gbyte ..... \$ 4000

Total CCD detector and data acquisition ..... \$ 152000

- *Cryogenic target*

- design and construction ..... \$ 30000

- material ..... \$ 20000

Total cryogenic target ..... \$ 50000

- *Installation on DAΦNE*

- thin beam pipe, mechanical supports, pumping, etc. ..... \$ 70000

Total installation ..... \$ 70000

- **Contingencies and other needs ..... $ 30000**

Global cost estimation of the DEAR experiment ..... $ 302000

9.2 Sharing of responsibilities

The groups of the DEAR Collaboration will share the responsibilities of the main items of the experiment in the following way :

- CCD detector: Neuchâtel group
- Cryogenic target: Tokyo groups
- Simulations and installation on DAΦNE: Frascati and Bucharest groups
- Tests, data taking, on-line analysis, off-line analysis: all groups

9.3 Time schedule

The DEAR experiment is able to perform background measurements from the first day a beam is circulating in the DAΦNE rings.

The experiment can be installed and eventually take data during the period of machine commissioning, because 3/4 of CCDs are ready and presently working at PSI, and the cryogenic target can be made in one year.

Duration of the installation of the set-up: two weeks.
Test and data taking:

- test runs and background measurements: two weeks
- data taking on kaonic hydrogen: 4000 events in the 6.5 keV peak, 20 X-rays/h at $L = 10^{32} cm^{-2} s^{-1}$; machine efficiency 80 % (injection every hour, duration 5 min): two weeks
- data taking on kaonic deuterium (same conditions): two weeks
- overall data taking time: 1 month
- If $L = 5 \cdot 10^{31} cm^{-2} s^{-1}$ (commissioning period) overall data taking time: 2 months

Overall requested time (installation, background tests, data taking, contingencies): 3 months

Acknowledgements

We wish to thank the Director of Frascati Laboratories, Prof. E. Iarocci, for the continuous encouragements and the useful discussions.

We are very grateful to the Director of $DA\Phi NE$ Machine Project, Dr. G. Vignola and to Dr. S. Guiducci for the helpful discussions and their support by providing us essential information on the $DA\Phi NE$ performance.

We acknowledge Dr. F. Nichitiu for his essential role played at the birth of the Proposal, bringing to our attention the fascinating case of the kaonic hydrogen puzzle.

Finally, we acknowledge Mrs. D. Pierluigi who made the editing of the Proposal with skilfulness and patience.